JGR Solid Earth

RESEARCH ARTICLE
10.1029/2024JB031053

Interconnectivity of Magmatic and Hydrothermal Systems of Aluto Volcano in the Main Ethiopian Rift Inferred From Seismicity

Tesfahiwet Yemane[1], Thomas Samuel Hudson[1,2], John Michael Kendall[1], Jonathan Blundy[1], Amdemichael Zafu Tadesse[1,3], James O. S. Hammond[4], Atalay Ayele[5], Ghebrebrhan Ogubazghi[6], and Sacha Lapins[7]

[1]Department of Earth Sciences, University of Oxford, Oxford, UK, [2]Department of Earth Sciences, ETH Zurich, Zurich, Switzerland, [3]School of Earth Sciences, Addis Ababa University, Addis Ababa, Ethiopia, [4]School of Natural Sciences, Birkbeck, University of London, London, UK, [5]Institute of Geophysics, Space Science and Astronomy, Addis Ababa University, Addis Ababa, Ethiopia, [6]Department of Earth Sciences, Eritrea Institute of Technology, Mai Nefhi, Eritrea, [7]School of Earth Sciences, University of Bristol, Bristol, UK

Key Points:

- Seismicity beneath Aluto reaches 40 km bsl but is negligible below the Silti Debre Zeyt Fault Zone which was previously interpreted as melt
- Focal mechanisms show normal faulting in the direction of rift extension and display double-couple mechanisms
- High b-values in Aluto suggest the presence of fluids, and that the magmatic and hydrothermal systems appear to be connected

Correspondence to:
T. Yemane,
tesfahiwet.abraha@sjc.ox.ac.uk

Citation:
Yemane, T., Hudson, T. S., Kendall, J. M., Blundy, J., Tadesse, A. Z., Hammond, J. O. S., et al. (2025). Interconnectivity of magmatic and hydrothermal systems of Aluto volcano in the Main Ethiopian Rift inferred from seismicity. *Journal of Geophysical Research: Solid Earth*, *130*, e2024JB031053. https://doi.org/10.1029/2024JB031053

Received 23 DEC 2024
Accepted 12 JUN 2025

Author Contributions:
Conceptualization: Tesfahiwet Yemane, John Michael Kendall
Data curation: Tesfahiwet Yemane, John Michael Kendall, Atalay Ayele
Formal analysis: Tesfahiwet Yemane
Funding acquisition: John Michael Kendall
Investigation: Tesfahiwet Yemane
Methodology: Tesfahiwet Yemane, Thomas Samuel Hudson, John Michael Kendall, Sacha Lapins
Project administration: John Michael Kendall
Resources: John Michael Kendall
Software: Thomas Samuel Hudson
Supervision: John Michael Kendall, Jonathan Blundy
Writing – original draft: Tesfahiwet Yemane

Abstract Aluto volcano, situated in the central Main Ethiopian Rift (MER) within the northern part of the East African Rift System (EARS) is seismically active, with indications of unrest detected by InSAR. It hosts Ethiopia's first pilot project for geothermal energy. Despite extensive studies, uncertainties remain about the mechanisms of unrest and the existence of a shallow magma chamber beneath Aluto which could drive the hydrothermal system, and is crucial for understanding its geothermal potential. This study investigates Aluto's magmatic and hydrothermal systems using observations of seismicity in the region. We analyze seismic data from January 2012 to January 2014, locating 2,393 events, which lie predominantly along the Wonji Fault Belt (WFB). Event depths reach up to 40 km beneath Aluto, suggesting the presence of a highly crystallized body at shallow depth, consistent with previous magnetotelluric and gravity studies. Deep crustal seismicity likely relates to fluid and/or magmatic processes. High b-values of 1.97 ± 0.10 at Aluto indicates the presence of fluids. Seismicity is negligible beneath Silti Debre Zeyt Fault Zone (SDFZ), previously identified as a highly conductive, indicative of melt. Focal mechanisms show normal faulting in the direction of rift extension and full-moment tensor inversions suggest shear-failure with fluids potentially activating existing faults. We suggest that the magmatic and hydrothermal systems are connected through pre-existing faults. Understanding this interaction will enhance our knowledge of the geothermal system, volcanic risk, mechanisms of unrest, and emplacement of geothermal brines.

Plain Language Summary Understanding the interaction between molten rock and hot water beneath a volcano is crucial to forecasting eruptions, harnessing geothermal energy, and finding metal-rich brines. Molten rock drives the circulation of hot fluids below the surface, which can be sources of geothermal energy and minerals. In this study, we use seismic data to assess the interaction between molten rock and hot fluids at Aluto. Aluto, showing signs of unrest, hosts a significant geothermal field but uncertainties remain about the cause of this unrest and the presence of molten rock at shallow depths. We located 2,393 earthquakes from January 2012 to January 2014. Earthquake depths extend up to 40 km below Aluto. Deep earthquakes are likely caused by fluids and/or molten rock movements. Earthquakes are negligible under Silti Debre Zeyt Fault Zone (SDFZ), indicating the presence of molten rock. A high ratio of small to large earthquake magnitudes at Aluto suggests the presence of fluids. Molten rock is connected to fluid circulation beneath Aluto through faults. Understanding this interaction can enhance our understanding of the geothermal system, volcanic risk, and metal-rich fluids.

1. Introduction

Volcanic complexes frequently experience unrest and occasional eruptions, making them difficult to predict and understand (Hutchison, Biggs, et al., 2016; Manley et al., 2021). Episodes of uplift and subsidence, marked by unrest, can occur with or without eruptions. These fluctuations are influenced by intricate mechanisms that encompass magma dynamics, geothermal systems, and tectonic stress (Acocella et al., 2015; Troise et al., 2019). However, understanding the interactions between these mechanisms and magmatic and hydrothermal systems is limited (Pritchard et al., 2019) due to their complexity, challenges in detailed crustal studies (Gauntlett

Writing – review & editing: Thomas Samuel Hudson, John Michael Kendall, Jonathan Blundy, Amdemichael Zafu Tadesse, James O. S. Hammond, Atalay Ayele, Ghebrebrhan Ogubazghi, Sacha Lapins

et al., 2023), and the lack of comprehensive descriptions of volcanic edifices on large scales (Gresse et al., 2021). Understanding this interplay is crucial for forecasting eruptions (Stix, 2018) and inferring unrest mechanisms (Roman et al., 2019). Additionally, it is essential for the successful exploration and production of geothermal energy (Heřmanská et al., 2019; Jolie et al., 2021; Okamoto et al., 2019; Reinsch et al., 2017; Samrock et al., 2023) and for locating and understanding the characteristics of metal-rich brine reservoirs (Blundy et al., 2021; T. Hudson et al., 2023; Sanjuan et al., 2022) hosting metals such as lithium (Weinand et al., 2023) or other hydrothermal deposits (Hedenquist & Lowenstern, 1994). Furthermore, understanding the location and mechanism of melt storage in the crust and upper mantle provide insights into magmatic systems and the process of rift evolution (Chambers et al., 2021).

Seismicity can provide insights into magma chambers and conduits (Segall, 2013) and the interaction between magma bodies, hydrothermal systems and their surrounding rocks (Wilks et al., 2020). In this study, we assess the interactions between hydrothermal and magmatic processes at Aluto volcano in the Main Ethiopian Rift (MER) and compare it to other previous volcanotectonic studies of the MER. Aluto is ideal due to indications of unrest, as identified through InSAR (Albino & Biggs, 2021; Biggs et al., 2011). Additionally, Aluto hosts a significant geothermal field that has been and continues to be explored through drilling, enabling us to establish constraints on the subsurface structure (Cherkose & Mizunaga, 2018; Gianelli & Teklemariam, 1993; Gizaw, 1993; Hochstein et al., 2017; Hutchison, Biggs, et al., 2016; Mulugeta et al., 2021; Pürschel et al., 2013; Saibi et al., 2012; Samrock et al., 2023; Teklemariam et al., 1996).

The MER is a volcanotectonic rift that signifies the center of continental stretching occurring between the Nubian and Somalian plates (Calais et al., 2006; Greenfield et al., 2019a; Wilks, Ayele, et al., 2017; Wilks, Kendall, et al., 2017). It is a volcanically active region in the northern part of the East African Rift System (EARS) (Bonini et al., 2005; Lavayssière, Greenfield, et al., 2019), and is known for hosting silicic volcanic complexes (Fontijn et al., 2018; Tadesse et al., 2023). The magmatic and tectonic history of the MER has traditionally been described using polyphase rifting models (Boccaletti et al., 1998; Bonini et al., 1997; Corti et al., 2003). However, recent studies indicate that the MER has experienced consistent oblique rifting over the past 11 Myr, which contradicts the polyphase rifting models (Agostini, Marco, Giacomo, Federico, & Francesco, 2011; Corti, 2008, 2009; Robertson et al., 2016). Rift evolution in the MER varies along the axis, with an early stage of evolution in the south progressing toward incipient breakup in the north. Consequently, the distribution and style of Quaternary volcanotectonic deformation is well known in the north compared to the south, where it is less constrained (Agostini, Marco, Giacomo, Federico, & Piero, 2011). The central part of the MER plays a crucial role in assessing the overall volcanic and tectonic development of the EARS (Woldegabriel et al., 1990). It comprises the mid-Miocene border faults and the recent Quaternary in-rift faults named as the Wonji Fault Belt (WFB) (Keir et al., 2015).

The Aluto volcanic complex is a silicic peralkaline volcano located in the central part of the MER, with few details known about its eruptive history (Hutchison, Pyle, et al., 2016). Recent volcanism in Aluto covers an area of approximately 8 km in diameter (Hutchison, Pyle, et al., 2016). The structure and volcanic evolution of the Aluto volcanic complex is controlled by the influence of the NNE-trending WFB (Le Turdu et al., 1999). Several recent investigations have been conducted to assess the Aluto volcanic complex, including various geological, eruptive history, geochemical (Hutchison, Fusillo, et al., 2016; Hutchison, Pyle, et al., 2016; McNamara et al., 2018; Regenspurg et al., 2022; Woldegabriel et al., 1990), geophysical (Cherkose & Mizunaga, 2018; Mulugeta et al., 2021; Nigussie et al., 2023; Nowacki et al., 2018; Samrock et al., 2015; Wilks, Kendall, et al., 2017; Wilks et al., 2020), and geothermal development (Gizaw, 1993; Jolie et al., 2019; Teklemariam et al., 1996) studies. The Aluto-Langano geothermal field is the sole operational site for geothermal energy in Ethiopia (Benti et al., 2023) with high enthalpy and salinity levels (Pürschel et al., 2013), and it is the most extensively investigated prospects in the MER (Samrock et al., 2020). Despite Aluto being extensively studied, uncertainties persist about mechanisms of unrest, fluid distribution in the subsurface and ascent along mapped fault zones, crucial for understanding its geothermal system (Jolie et al., 2019). In addition, it is also unclear whether there is a very shallow magma reservoir beneath Aluto volcano. Some studies suggest that, it is unlikely, attributing the source of unrest to fluctuations in the hydrothermal system instead of a magmatic system (Samrock et al., 2015, 2023). On the contrary, other observations indicate the presence of a shallow and frequently replenished magma storage zone (Biggs et al., 2011; Gleeson et al., 2017; Wilks, Kendall, et al., 2017).

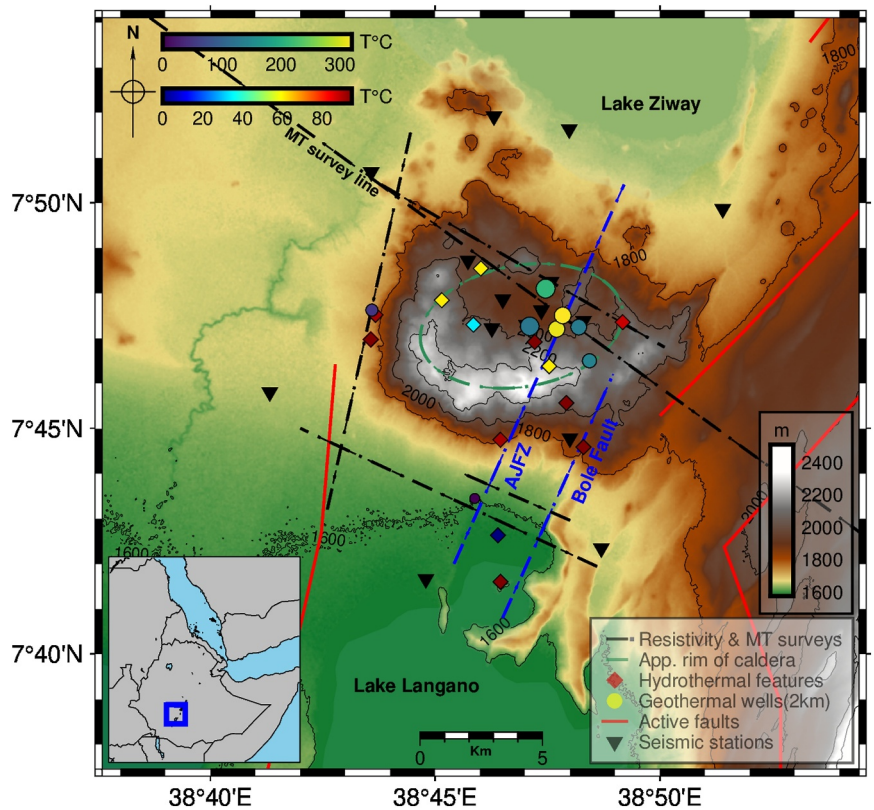

Figure 1. Aluto volcano, with its caldera rim indicated by a green dashed ellipse. The XM network stations from the ARGOS experiment are represented by black inverted triangles. Hydrothermal features are depicted as diamond shapes, colored by temperature. Geothermal wells are shown as circles, also colored by temperature and sized by well depth (Hutchison et al., 2015). Resistivity and magnetotelluric surveys conducted for geothermal exploration are represented by black dashed lines (Hochstein et al., 2017). The Bole fault and Artu Jawa Fault Zone are marked by blue dashed lines and active faults by red solid lines (Styron & Pagani, 2020).

Here we use seismicity to investigate the magmatic and hydrothermal systems of Aluto and interpret the results in the context of previous geophysical and geological knowledge of the Aluto volcano. We reanalyze seismic data sets from Aluto volcano recorded from January 2012 to January 2014. In the previous study, seismic events were detected and located using primary (P-) and secondary (S-) wave picks at individual stations (Wilks, Kendall, et al., 2017). In this study, we apply a back-migration detection method that allows for the detection of events closer to the noise threshold, theoretically enabling a more comprehensive study of seismicity. We also calculate earthquake moment magnitudes, b-values and source mechanisms to better understand the hydrothermal and magmatic systems of Aluto.

2. Data and Methods

The data for this study are from a network of 12 Güralp CMG-6TD 30 s three-component seismometers located on the volcanic edifice and its surrounding rift valley floor, covering 20 × 20 km area with station spacing ranging from 2 to 10 km. The seismic network was deployed between 08 January 2012 and 31 January 2014 with the XM Network (The ARGOS Project, 2012), shown by black inverted triangles in Figure 1. Data are sampled at 100 Hz.

2.1. Earthquake Detection and Locations

Data from the XM network were used to detect and locate seismic events in Aluto using QuakeMigrate, an algorithm for microseismic detection (T. Hudson et al., 2019; Smith et al., 2020). This approach involves retroactively tracing the energy arriving at seismic stations, searching for the coalescence of energy from multiple stations in both time and space. The raw seismic waveforms for each station is bandpass filtered with high and low corners of 16 and 2 Hz. Short-Term-Average (STA) to Long-Term-Average (LTA) algorithm is then applied to

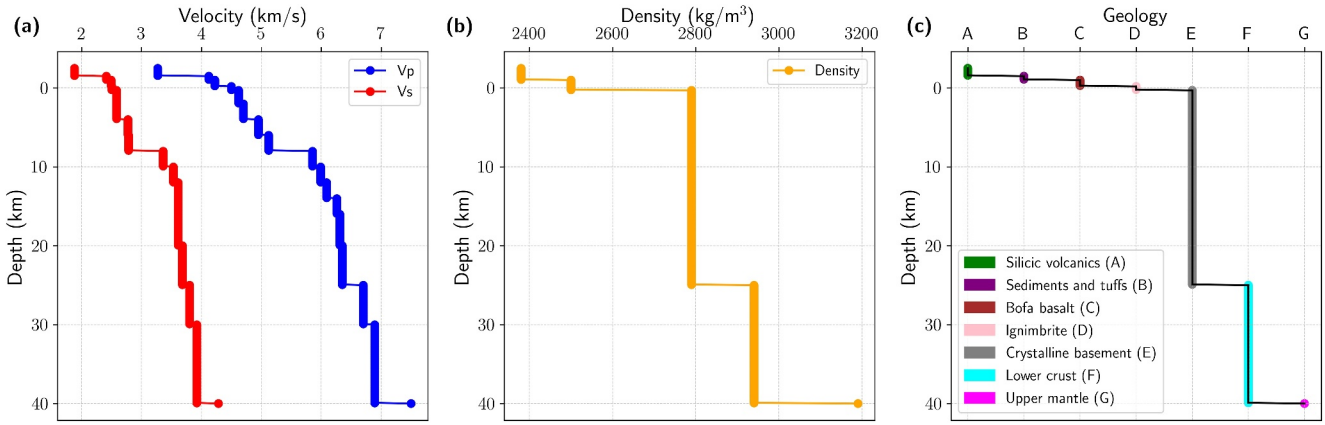

Figure 2. The input velocity model used for this study. (a) The input velocity model for P- and S-waves from Wilks, Kendall, et al. (2017). (b) The density of the rocks versus depth beneath Aluto (Cornwell et al., 2006; Wilks, Kendall, et al., 2017). (c) The inferred geology versus depth, color-coded and labeled from A to G.

generate the onset function. Onset functions for each seismic station were obtained using an STA (0.2s) to LTA (1.0s). The primary wave onset function is determined from the vertical component, and the secondary wave onset function is derived from the horizontal components. These onset functions from each station are then combined and moved through time and space to look for a coalescence of energy from the combination of peaks seen in the onset functions of individual stations. An event is triggered when the maximum coalescence energy value at a particular point in 3D space at a given time is very high. The onset function can be estimated by a Gaussian distribution (Drew et al., 2013). The estimated arrival time picks are the peak of the onset function and the associated uncertainty is calculated as the standard deviation around this peak (Smith et al., 2020). The initial locations of the earthquakes are detected using this method, resulting in 3,401 events.

We use the non-linear location method (Lomax et al., 2000) to relocate the events detected using the traveltime formulation for P- and S-phases (Podvin & Lecomte, 1991). This method employs efficient global sampling algorithms to estimate the 3D posterior Probability Density Function (PDF) for earthquake hypocenter locations (Lomax, 2005). This PDF, following probabilistic earthquake location methods by Tarantola and Valette (1982), Moser et al. (1992) and Wittlinger et al. (1993), provides a detailed representation of likely hypocenter locations with comprehensive uncertainty information. The Oct-tree method is used here to determine the location of PDFs and likelihood hypocenters (Lomax & Curtis, 2001) and the velocity model used for this study is shown in Figure 2. We relocated 2,393 events as shown in Figure 3 with phase numbers greater than four and reduced spatial errors in the event locations.

2.2. Earthquake Magnitudes

2.2.1. Moment Magnitude (Mw)

Earthquakes are measured by their energy release, with magnitude indicating their size. Richter (1935) introduced local magnitude (M_L) as the first scale to numerically characterize an earthquake size. Most magnitude scales rely on seismogram amplitudes, signal duration and frequency-domain measurements (Ottemoller & Havskov, 2003) which give empirical measures (T. Hudson et al., 2022). Moment magnitudes defined by Kanamori (1977), are grounded in physical principles based on rupture models like Brune model (Brune, 1970). This allows moment magnitude to quantify earthquakes of various types and magnitudes accurately (Deichmann, 2006; Uchide & Imanishi, 2018). Here, to determine earthquake magnitudes, we use the moment magnitude scale, which is calculated by fitting a Brune model (Brune, 1970) to the earthquake spectra. T. Hudson et al. (2022) and Stork et al. (2014) have shown the robustness of using moment magnitude. We selected 1,262 events recorded by at least four stations, each with a minimum of two P-phase and two S-phase picks.

2.2.2. B-Values

The Gutenberg-Richter distribution is represented as:

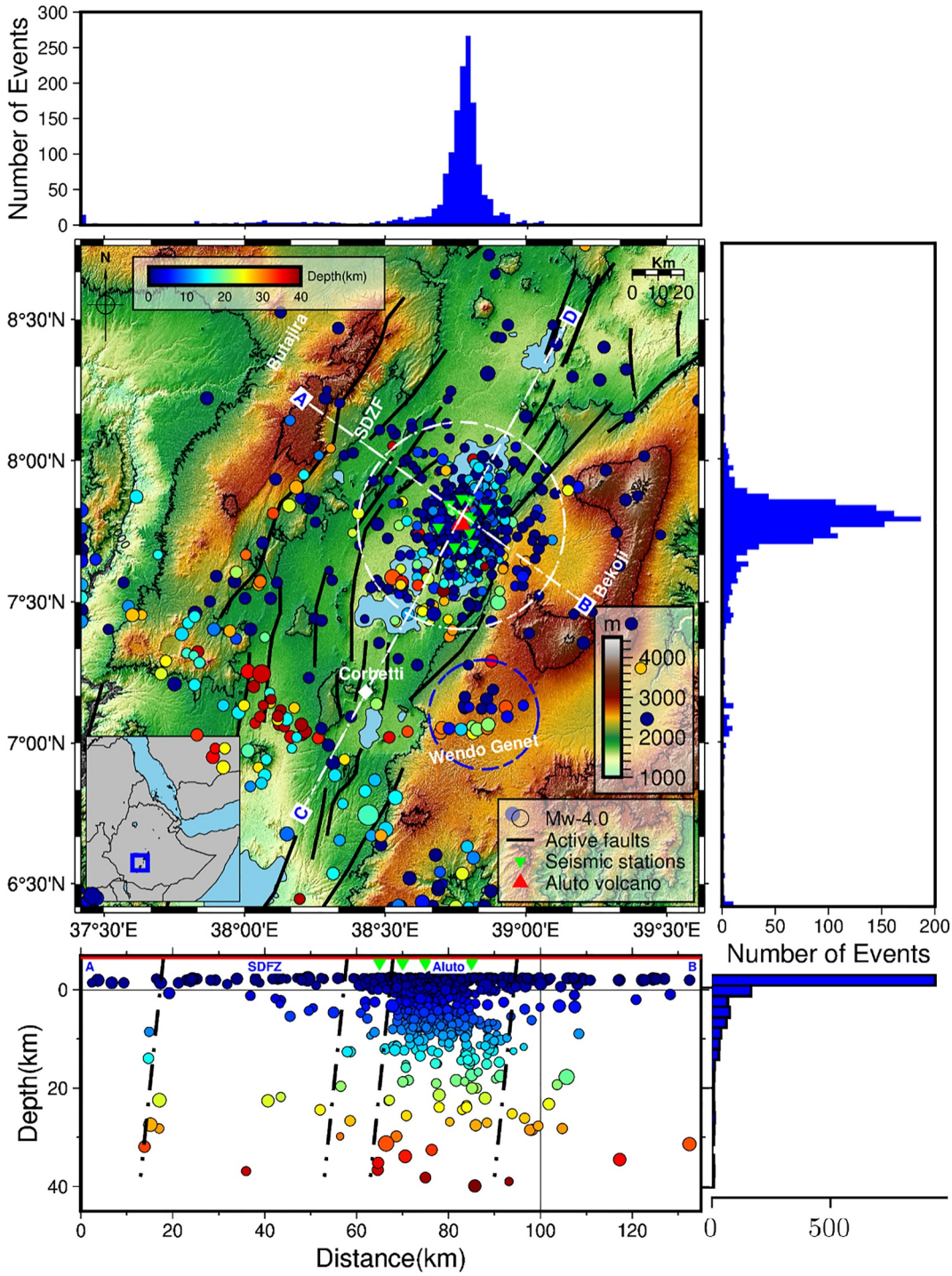

Figure 3. Seismic activity at Aluto and around Aluto from January 2012 to January 2014. The depth profile along the white dashed line from A to B is presented at the bottom. The distribution of events by longitude is shown on the top side, while latitude distribution is displayed on the right side. Aluto caldera is marked by a red triangle within the circular dashed white circle, while seismometers are indicated by green inverted triangles. Events are color-coded according to their depth and scaled by moment magnitude. Active faults are represented by black lines (Styron & Pagani, 2020). Additionally, the black dashed lines at the bottom of the figure represent faults, and the depth distribution of events is detailed in the same panel. Events occurring in Wendo Genet are enclosed within a blue dashed circle.

$$\log_{10} N = a - bM, \quad (1)$$

and characterizes the magnitude-frequency distribution of earthquakes in a specific region (Gutenberg & Richter, 1944), where N is the number of earthquakes equal to or exceeding magnitude M, while a and b denote constants that describe the rate of seismic activity and the relationship between the rate of smaller and larger earthquakes, respectively. The b-value, observed to be varying in space and time (Shelly et al., 2016; Taroni et al., 2021), reflects changes in crustal stress (El-Isa & Eaton, 2014; Wyss, 1973). It also serves as an indicator of conditions like faulting style (Petruccelli et al., 2019), strength heterogeneity (De Gori et al., 2012) and fluid pressure (Bachmann et al., 2012; Shelly et al., 2016), contributing to a better understanding of seismicity (Herrmann et al., 2022).

Here we compute the b-values using the boundary-value-stability (Roberts et al., 2015), determining individual b-values through the maximum likelihood method. We used the same number of events as those used for the moment magnitude in the b-value calculations.

2.3. Moment Tensor Inversion

Seismic signals provide details about the earthquake moment tensor (J. Hudson et al., 1989) and the decomposition of moment tensors into different components helps to classify and understand seismic source mechanisms (Chapman & Leaney, 2012; Stich et al., 2003; Vavryčuk, 2015). These mechanisms are determined by analyzing the initial motion directions of P-waves and amplitude ratios recorded at nearby seismic stations (Hardebeck & Shearer, 2002, 2003). These far-field first arrival polarities are less affected by uncertainty in the velocity model than absolute amplitudes used in full-waveform source mechanism inversions (Pugh et al., 2016). Here we compute full moment tensor and double-couple constrained inversion using P polarity using a Bayesian method approach, MTfit (Pugh et al., 2016; Pugh & White, 2018). The events selected for moment tensor inversions are based on an azimuthal gap of less than 180°, at least six P-wave arrivals, an RMS travel-time residual (t_{RMS}) of less than 1 s, and a depth uncertainty of less than 3 km, as shown in Figure 6.

3. Results

Using the XM network at Aluto volcano and its surroundings, we identified 2,393 earthquakes using the nonlinear location method. Figure 2 shows the model of P- and S-wave velocities used in this study, which were obtained from well-log data and travel-time inversions in the northern MER (Wilks, Kendall, et al., 2017). Figure 3 illustrates the seismicity of Aluto volcano (2,393 events), with events extending up to 40 km beneath Aluto. The profile from A to B is along the same line of the earlier magnetotelluric survey done by Hübert et al. (2018), were they located melt below SDFZ, at 40–50 km northwest of Aluto at a depth of 10–12 km bsl. We show that this region also has negligible seismicity, as indicated in Figure 3. The majority of events at Aluto are shallow depth and are located at the center of the caldera and the seismic activity aligns parallel to the existing Artu Jawa Fault Zone (AJFZ) and SDFZ faults.

Figure 4 shows the seismicity and daily average moment magnitude in Aluto, revealing temporal variations in seismic behavior similar to the works of Birhanu et al. (2018) using seismicity and GPS station data. There are more events in October and November in both 2012 and 2013. The peak of seismic activity occurs 2–3 months following the rainy season, which lasts from July to September, and decreases during the dry seasons. Figure 4 also shows the frequency distribution of moment magnitude, for Aluto. The b-value at Aluto is 1.97 ± 0.10 and similar observations were reported by Wilks, Kendall, et al. (2017).

The event locations are consistent with those reported by Wilks, Kendall, et al. (2017), as shown in Figure 5. However, we significantly improved the t_{RMS} and azimuthal gap in this study. Most events in this study have a t_{RMS} of less than 1 s, as indicated by the vertical dashed black line in Figure 5e. Additionally, most events have an azimuthal gap of less than 180°. We also considered a minimum of four phases per event, and the spatial errors for most events are relatively acceptable. In the cross-section of longitude and latitude versus depth (Figures 5c and 5d), there is an umbrella-like structure at a greater depth.

The seismic activity at the Aluto caldera is shown in Figure 6, where events are selected based on a t_{RMS} of less than 1 s, an azimuthal gap of less than 180°, a minimum of four phases, and spatial errors with X (longitude) and Y

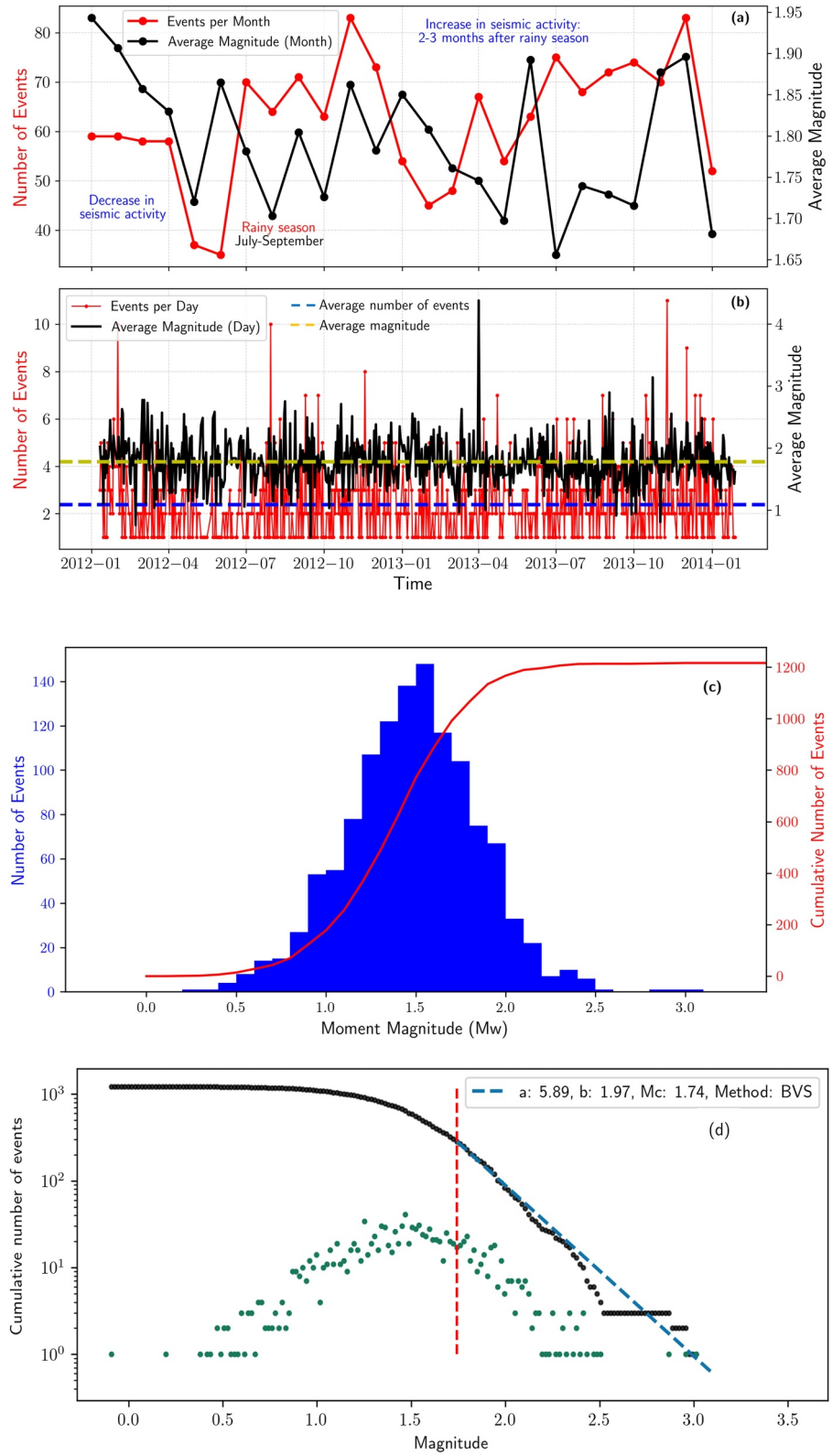

Figure 4.

(latitude) errors of less than 10 km and Z (depth) errors of less than 5 km as shown in Figures 5e–5h by black dashed vertical lines. Most of the events are shallow and are located around the caldera. The distribution of events appears to follow the NE-SW trending faults (AJFZ) and areas with significant hydrothermal vent manifestations. This is more evident in Figures 6b and 6c, which show the cross-sections of depth versus latitude and longitude, where most of the events follow the fault trend from a certain depth to near the surface. Hydrothermal vents are prominent along fault lines and the rims of the caldera (Hutchison et al., 2015), where we have more events. The temperature of hydrothermal features is also highest along these fault lines and caldera rims, where geothermal wells have been drilled (Hochstein et al., 2017). These areas also exhibit elevated CO_2 release along the faults (Hunt et al., 2017). Lower crust seismicity is common in the MER, and Figure 7 shows the profile from C to D in Figure 3 in which the seismicity extends up to 40 km bsl. The right panel (c and d) in Figure 7 shows similar lower crust seismicity studies by Lapins et al. (2020) in Wendo Genet region to the south of Aluto.

We perform both full moment tensor and double-couple constrained source mechanism inversions. Figure 8 displays lune plots (Tape & Tape, 2012), illustrating mechanisms that are near double-couple. The focal mechanisms shown in Figure 8 predominantly exhibit normal faults with small strike-slip components that align with the existing fault orientations. The focal mechanisms of the MER are dominated by normal faulting with a small component of left-lateral strike-slip (Ayele, 2000).

The seismic events along the profile from A to B in Figure 3 are overlaid on previous magnetotelluric (Dambly et al., 2023) and gravity (Cornwell et al., 2006) studies in Figure 9. This profile follows the same magnetotelluric survey line as in Hübert et al. (2018), which identified a high conductor below the SDFZ at depths of 10–12 km bsl, interpreted as melt. Additionally, they identified a highly resistive body beneath Aluto, interpreted as a mafic gabbroic intrusion. The gravity survey reveals a high-density gabbroic body below the rift axis with densities similar to those calculated for cumulates using Rhyolite-MELTS (Hutchison et al., 2018) and lower densities off the rift axis, also interpreted as melt. In this study, the highly resistive and high-density body beneath Aluto corresponds to significant seismic activity, while the high conductor region with slightly lower density beneath the SDFZ exhibits negligible seismicity.

Figure 10 illustrates the schematic 3D cross-section along the profile from A to B in Figure 3 with the rock types indicated. Pre-existing faults and fracture systems that extend deeper are serving as pathways connecting the magmatic and hydrothermal systems in Aluto, as depicted in the figure.

4. Discussion

4.1. Aluto Seismicity

The majority of the events beneath Aluto occur within the upper 2 km. Most of the events occur around the caldera and align with the NE-SW trending AJFZ, which cross-cuts the caldera edifice and ring faults. These areas are also characterized by hydrothermal vents and elevated CO_2 flux, as fluid pathways are structurally controlled. The highly fractured nature of the region enhances fluid saturation and permeability, facilitating the ascent of fluids along these faults, which can, in turn, trigger seismicity. There is also a seasonal pattern in seismicity and peaks at 2–3 months after the main rainy season which is between July and September. This is the time when the lake level of Ziway and Langano is high suggesting that precipitation has a role in replenishing the hydrothermal system. The highly fractured hydrothermal system region (Wilks, Kendall, et al., 2017) may facilitate this process. Therefore, the shallow events distributed around the caldera and along the fault trends are associated with hydrothermal activity in the shallow crust, as well as hydrological loading, as shown by Birhanu et al. (2018).

Seismicity is negligible to the northwest and northeast of Aluto. The network coverage in these areas is less sensitive. However, we suggest a more stable, seismically inactive crust in the northeast (e.g., there is no indication of elevated CO_2 flux (Hunt et al., 2017)) and the presence of melt in the northwest. Previous

Figure 4. Seismic activity from January 2012 to January 2014. (a) The average number of events per month and the corresponding moment magnitude. (b) The number of events per day and the average moment magnitude of events per day from January 2012 to January 2014. The blue dashed line is the average number of events over the entire period, while the yellow dashed line represents the average moment magnitude throughout the entire duration. (c) The number of earthquakes in each magnitude range. (d) Cumulative number of events plotted against moment magnitude in the Gutenberg-Richter plot. The moment magnitude (Mw) catalog is represented in black dots. The red dashed vertical line indicates the magnitude of completeness (Mc). The green dots show the values of individual bins for Mw. BVS denotes the b-value stability method employed for calculating the b-values. This figure provides values for Mc, as well as parameters a and b.

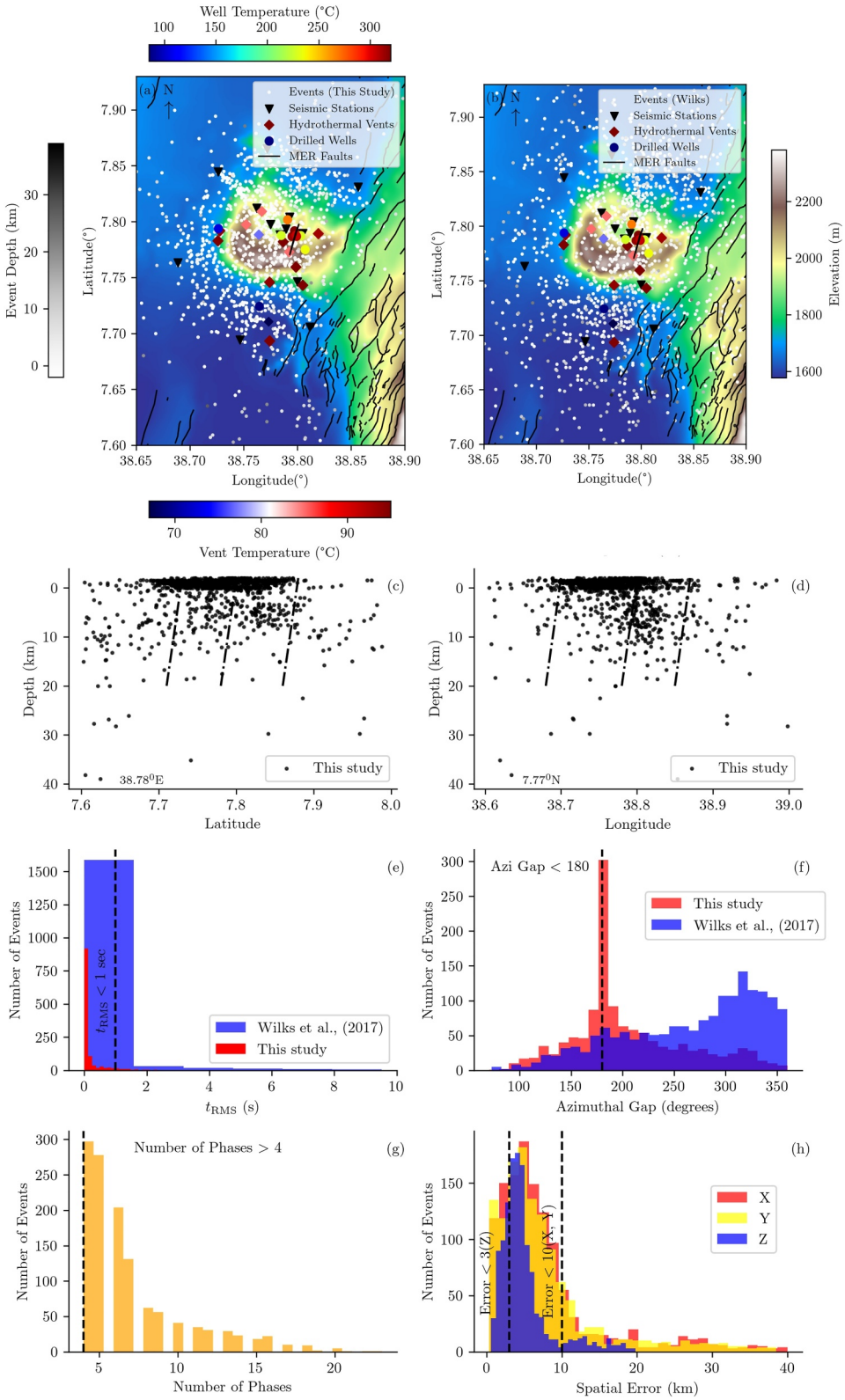

Figure 5.

magnetotelluric and gravity studies indicated that the melt lies approximately 40 km northwest of Aluto, beneath the SDFZ, and an intrusive body beneath Aluto. The presence of melt beneath the SDFZ is supported by negligible seismic activity in this study. However, seismicity is observed as a planar feature along the fault structure to the west of the SDFZ as shown in Figure 3. Moreover, seismic activity extending up to 40 km beneath Aluto supports the presence of an intrusive or highly crystallized mush with pockets of melt.

The depth of the events in Aluto extends up to 40 km bsl, that is into the lower crust and uppermost mantle. Earthquakes in the lower crust are common in continental rifts (Déverchère et al., 2001; Zhao et al., 1997). Nevertheless, the source of this activity is poorly understood (Chen & Molnar, 1983). In the MER, seismicity has been detected in the deep crust and upper mantle (Albaric et al., 2014; Lavayssière, Drooff, et al., 2019; Lindenfeld & Rümpker, 2011; Nyblade & Langston, 1995). The deep crustal seismicity are likely due to fluid and/or magmatic processes (Greenfield & White, 2015; T. Hudson et al., 2017; Lapins et al., 2020; Soosalu et al., 2010).

At these depths, the crust is typically ductile, so brittle failure requires a sufficiently high rate of strain release. We propose that the primary mechanism causing such rapid changes in strain rate is the ascent of fluids. In the ductile zone of the earth's crust, earthquakes occur when fluid moves through the rock rapidly enough to trigger brittle failure (T. Hudson et al., 2017). Moment tensor inversions could offer further validation of this interpretation, although we do not have such inversions for earthquakes occurring below 20 km. Moment tensor inversions at 5–10 km depth support the interpretation of seismic energy release mainly through brittle failure, but the presence of fluids (b-value >1) may contribute to fault activation. The lithospheric mantle has temperatures adequate to support partial melting (Hammond et al., 2014; Kendall et al., 2005) and this may not be caused by the slip of border faults. The earthquakes in the lower crust are triggered by magmatic activities in warmer, mafic lower crust (Keir et al., 2009). Based on limited observations, our preferred interpretation is that this deep seismicity is likely linked to the ascent of fluids along, critically stressed, fluid-rich faults.

4.2. Magmatic System

The seismicity beneath Aluto extends up to 40 km bsl, suggesting the absence of hot or too ductile body at shallow depth. The umbrella-like structure in Figures 5c and 5d is likely the top part of the magmatic mush beneath Aluto. However, it is deeper than what was previously thought in earlier studies (Biggs et al., 2011; Wilks, Kendall, et al., 2017). In an earlier seismicity study, deep crustal events were not observed and the seismicity beneath Aluto decreases after 9 km, which was interpreted as the existence of a magma mush at shallower depths (Biggs et al., 2011; Wilks, Kendall, et al., 2017). However, the current study observes seismicity beyond this depth. This finding is interesting as it provides evidence for the presence of a highly crystallized intrusive body or a highly crystallized mush with melt pockets at shallow depth.

The seismic activity directly beneath Aluto is consistent with imaging of Aluto from magnetotelluric imaging (Dambly et al., 2023; Hübert et al., 2018; Samrock et al., 2015, 2021; Whaler & Hautot, 2006), gravity (Mickus et al., 2007), resistivity (Hochstein et al., 2017), and velocity tomography (Daly et al., 2008; Mackenzie et al., 2005). Magnetotelluric and resistivity results (Dambly et al., 2023; Hübert et al., 2018; Samrock et al., 2015) show a high resistivity intrusive body beneath Aluto as shown in Figure 9. The magnetotelluric study of Samrock et al. (2021) shows that Aluto's upper crustal reservoir is cooler and more crystalline, with a higher magmatic volatile phase content at shallow depth. Moreover, the crustal magma beneath Aluto could have been cooled as the estimated time required for the cooling of crustal magma bodies of similar volume is approximately 100 ka, a duration, well within the post-caldera phase time frame of Aluto (Hübert et al., 2018). A gravity survey (Mickus et al., 2007) also detected a high-gravity anomaly in Aluto indicating a dense intrusion (Mulugeta et al., 2021; Searle & Gouin, 1972) and similar results were found at the Boku volcanic complex (Wuletawu

Figure 5. Seismic events zoomed at Aluto: (a) this study and (b) Wilks, Kendall, et al. (2017). Event depths are color-coded by depth, ranging from gray to black. Geothermal wells and hydrothermal vents are also indicated in panels (a) and (b). Main Ethiopian Rift faults are represented by black solid lines. Cross-sections of event depth versus latitude at 38.78°E (c) and depth versus longitude (d) at 7.77°N for this study are shown. Black dashed lines in the cross-sections represent inferred fault planes, interpreted from the spatial clustering and alignment of seismicity in map view. They are not to scale, do not represent actual depths, and are not constrained by focal mechanisms. Due to the N10°–20° fault orientations and the N–S or E–W orientation of the cross-sections, not all faults are fully represented in each view. (e) Shows the t_{RMS} of both studies, where the t_{RMS} in this study is significantly improved. (f) Illustrates the azimuthal gap for both studies, with the azimuthal gap in this study also showing considerable improvement. (g) and (h) present the total number of phases and spatial errors of the event locations in this study. Events with a minimum of four phases (that have two P- and S-waves) are used to select events for moment magnitude and b-value calculations.

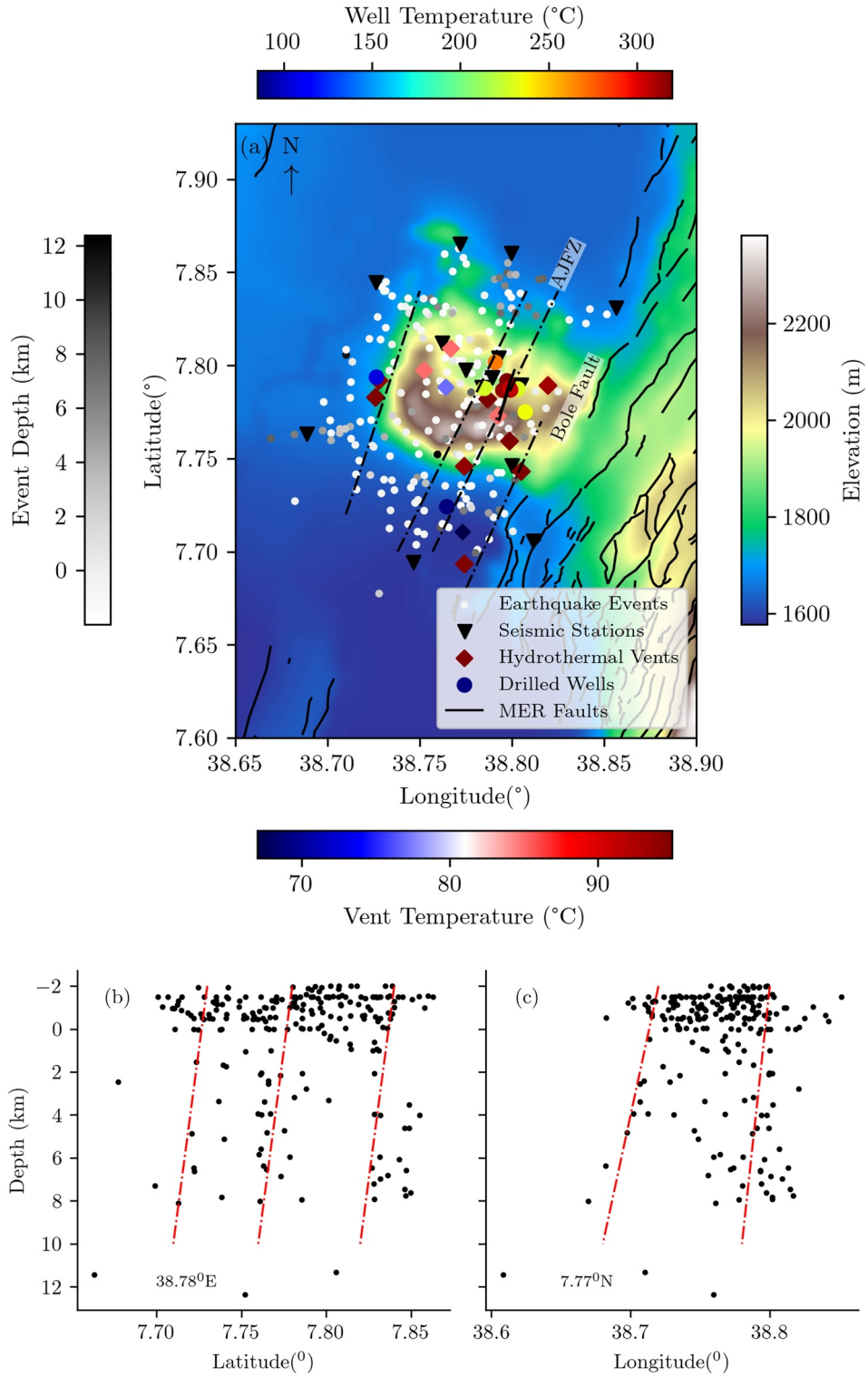

Figure 6. Seismic events at Aluto (a) filtered based on t_{RMS} less than one second, an azimuthal gap of less than 180°, a number of phases greater than four, and spatial errors of X (longitude) and Y (latitude) less than 10 km and Z (depth) less than 5 km, as indicated by black vertical lines in Figure 5. Earthquake events are colored by depth. Seismic stations are represented by black inverted triangles, hydrothermal vents by diamond shapes colored by temperature, and geothermal wells by circular markers, also colored by temperature. Black solid lines indicate Main Ethiopian Rift faults, while black dashed lines represent Artu Jawa Fault Zone (AJFZ) faults. Panels (b) and (c) display cross-sections along latitude at 38.78°E and longitude at 7.77°N, respectively. Red dashed lines indicate inferred fault planes based on seismicity patterns in map view. These are schematic, not to scale or true depth, and may not represent all mapped faults due to projection limits. The earthquake events align with the NE-SW trending AJFZ faults.

et al., 2024). Additionally, in the mid-to-upper crust, the velocity changes from 6.1 km/s on the rift flanks of the Ethiopian plateau to 6.6 km/s under the Quaternary magmatic segments suggesting the existence of aligned cooled gabbroic bodies along the rift axis (Maguire et al., 2006). Moreover, Daly et al. (2008) found a low Vp/Vs ratio at Aluto and the axis of the rift, interpreted as cooled mafic intrusions (Keranen et al., 2004) and wells drilled to a depth around 2 km bsl indicates no signs of melt (Gianelli & Teklemariam, 1993; Gizaw, 1993). Therefore, based on the new seismicity and other geophysical studies in Aluto, it is unlikely that there is a magma chamber at shallow depths. This finding contrasts with geological and geochemical studies (Hutchison, Biggs, et al., 2016). However, we suggest that a highly crystallized body with pockets of melt could exist. If the melt proportions are very low, such a body may be detected by magnetotelluric methods as a resistive structure (Hübert et al., 2018).

The absence of seismicity in the northwest of Aluto at SDFZ is consistent with earlier magnetotelluric and gravity studies as well as anisotropy and shear velocity studies of the MER. This may be linked to a melt or magma (Yirgu et al., 2006) reservoir at 10–12 km depth beneath SDFZ, as indicated by magnetotelluric results (Hübert et al., 2018). Additionally, Stuart et al. (2006) found a high Vp/Vs ratio beneath SDFZ indicating the presence of crustal melt which is consistent with the geochemical analysis of T. O. Rooney et al. (2005), T. Rooney et al. (2007). Other studies of anisotropy also show evidence of melt beneath the Ethiopian plateau (Bastow et al., 2010; Hammond et al., 2014; Keir et al., 2011; Kendall et al., 2006). The magmatic melt is located beneath the SDFZ, despite higher seismic activity in Aluto, particularly along the WFB. Dambly et al. (2023) indicated that magma moves at an angle toward the eastern WFB rather than rising vertically beneath the SDFZ and the structural controls influence the formation of the magmatic pathways. Although, recent volcanism has occurred near the western part of the rift along the SDFZ (Iddon & Edmonds, 2020; T. O. Rooney et al., 2005) and a significant flux of CO_2 is emitted in the Butajira region (Hunt et al., 2017). Additionally, there is a spatial correlation between the fault system at Aluto and the magma ascent channel (Dambly et al., 2023). This may be also attributed to the fact that 80% of the strain is in the WFB (Bilham et al., 1999; Ebinger & Casey, 2001) indicating that the WFB is more active than the SDFZ. Moreover, the magmatic plumbing system within the WFB is mature, allowing magma to quickly rise through existing conduits to fractionate at shallow depths while exhibiting fractionation throughout the crust in the SDFZ (T. O. Rooney et al., 2005; T. Rooney et al., 2007).

4.3. Hydrothermal System

The b-value at Aluto is 1.97 ± 0.10. The b-values in a tectonic setting are typically around 1.0 (Frohlich & Davis, 1993). However, higher b-value have been observed in volcanic areas (Bridges & Gao, 2006; Greenfield et al., 2020; McNutt, 2005; Wyss et al., 2001), often linked to a decrease in effective normal stress caused by the presence of fluids (Greenfield et al., 2019b; T. Hudson et al., 2022; Vavryčuk, 2001, 2002). The high b-value at Aluto, therefore, suggests the presence of fluids, although temperature or other factors could play a role. These fluids are mainly exsolved fluids of magmatic nature as there is high magmatic volatile phase content at shallow depth (Samrock et al., 2021). Consequently, the magmatic reservoir is connected to the hydrothermal system at Aluto as faults and fractures intersect shallow dikes or magma storage regions (T. Rooney et al., 2007). This is illustrated in Figures 5c and 5d, which show an umbrella-shaped structure of the magmatic body with faults extending to its top part. In Tullu Moye, similar to Aluto, faults facilitate the ascent of fluids of magmatic origin to the surface from depths of around 14 km (Samrock et al., 2018) and fault structures and hydrothermal activity overlap with the sill's surface projection (Kebede et al., 2023). Faults serve as channels for magma and fluid movement, while some extending to the upper mantle to facilitate the ascent of mafic melts, while others reached magmatic reservoirs where differentiated magma was stored (Boccaletti et al., 1999), as observed at Gedemsa (Peccerillo et al., 2007). Post-caldera vents (Lloyd et al., 2018), basaltic scoria cones and their related lava flows are also aligned along faults and extensional features (Hunt et al., 2020). Additionally, the distribution of earthquake hypocenters, as well as volcanic vents, are clustered (see Figure 6), which is consistent with Mazzarini et al. (2013), indicating that faults are pathways for fluid ascent. In rift systems characterized by high volcanic and seismic activity, existing faults could govern magma ascent and eruption and influence the movement of hydrothermal fluids and gases (Hutchison et al., 2015). Both regional and caldera structures serve as pathways for hydrothermal fluids, making them vital for geothermal exploration. Caldera faults in particular could enhance permeability upon reactivation, potentially concentrating hydrothermal fluid flow and becoming prime areas for intercepting fluids (Maestrelli et al., 2024).

Sampling CO_2 emissions from fumaroles in Aluto has revealed that the magmatic and hydrothermal systems are interconnected by faults and fractures (Hutchison, Biggs, et al., 2016). The temperature of the hydrothermal

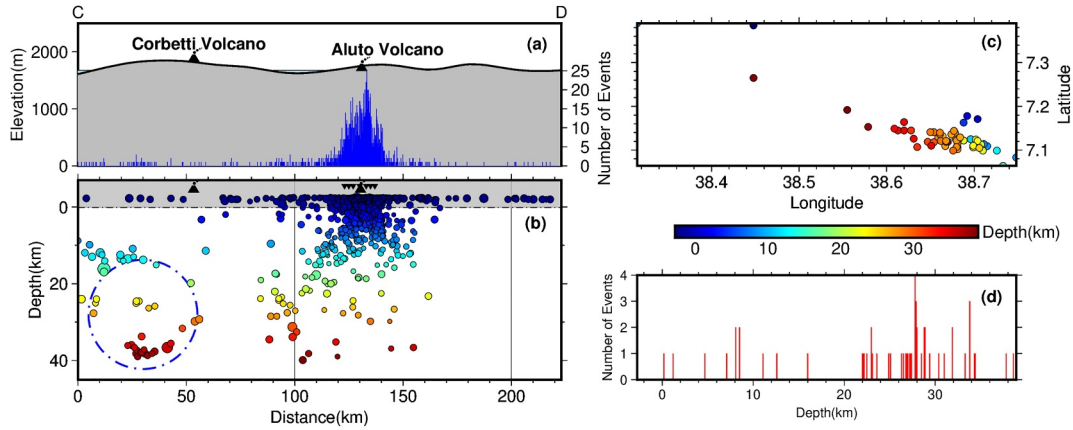

Figure 7. Seismic activity along the profile from C to D in Figure 3. (a) Distribution of events along the white dashed line extending from point C to D. (b) Depth profile along the same line, with events in Wendo Genet highlighted within the blue dashed circle. (c) The seismic activity in the lower crust of Wendo Genet (Lapins et al., 2020), as indicated in part b. (d) The depths of the events mentioned in part c.

features is highest along the fault lines (Figure 1) and increases toward the center of Aluto, indicating that these faults likely serve as pathways (e.g., AJFZ (Nowacki et al., 2018)) for the fluid movement. CO_2 degassing is primarily concerned along faults (Hunt et al., 2017). Enhanced degassing along fault and fracture systems show deep permeable segments of active faults indicating significant areas for the movement of hydrothermal fluids (Jolie et al., 2019). Therefore, the pre-existing faults and fracture systems act as pathways that connect the magmatic system with a shallow hydrothermal system (Wilks et al., 2020). The hydrothermal system in Aluto is therefore driven by the ascent of magmatic fluids through a fault and fracture systems and precipitation.

4.4. Causes of Unrest

We observed a significant peak in seismicity 2–3 months after the main rainy season at Aluto, coinciding with high lake levels of Ziway and Langano, indicating hydrological loading as the main cause of shallow seismicity. Seasonal seismicity in Aluto is linked to changes in surface loading and reservoir pore pressure, with fluid pathways controlled by structures like the AJFZ (Birhanu et al., 2018). Similar observations have been observed

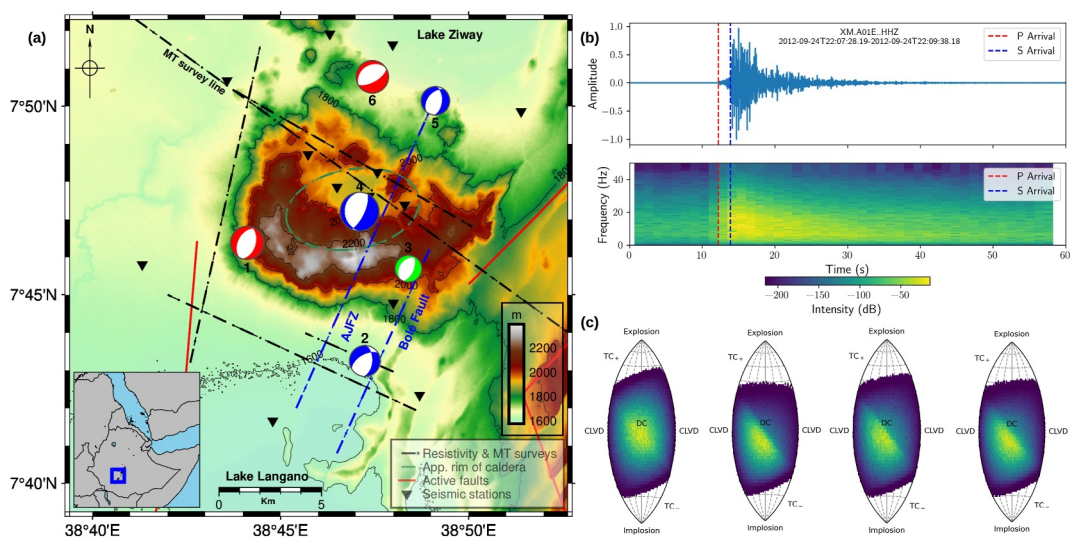

Figure 8. Focal mechanisms and lune plots illustrating the source Probability Density Function (PDF) for selected earthquakes around Aluto caldera. The events are located near the center of the network stations at a depth of around 5–10 km. (a) The focal mechanisms for six events numbered from 1 to 6. (b) The actual waveform and the spectrogram for event 2 at one of the stations. (c) The source PDF corresponds to the full moment tensor solution for events 1, 2, 4, and 5.

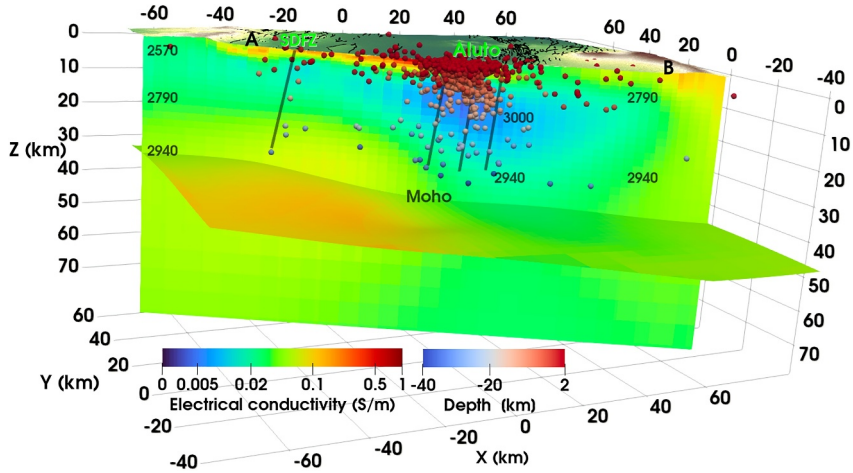

Figure 9. The 3D cross-section along the profile from A to B in Figure 3 depicts seismicity overlaid on the magnetotelluric survey conducted in a previous study by Dambly et al. (2023). The numbers in the figure indicate the subsurface density in kg/m^3 (Cornwell et al., 2006; Mickus et al., 2007) and vertical lines represent faults. High electrical resistivity and density is observed below Aluto compared to the surrounding area, with significant seismicity in this study extending up to 40 km bsl. A high conductivity body is detected beneath the SDFZ, consistent with results from other magnetotelluric and gravity studies not shown here. The study by Hübert et al. (2018) also reveals an even shallower conductive body beneath the SDFZ. The seismic activity is negligible beneath the SDFZ.

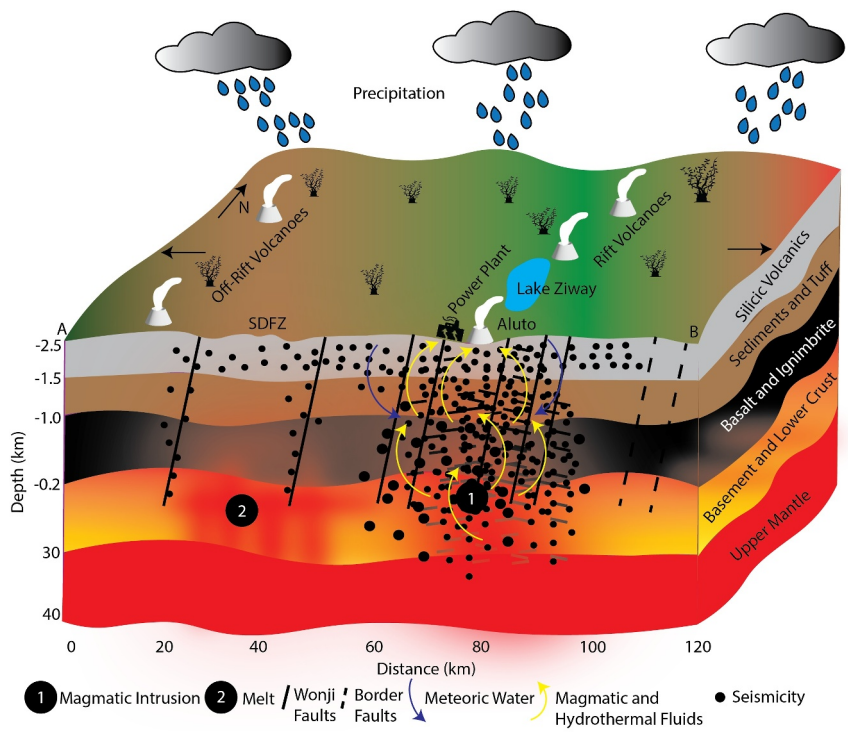

Figure 10. The schematic 3D cross-section along the profile from A to B in Figure 3 depicts different lithologies and structures. The rock types of the upper crust are vertically exaggerated (not to scale). The melt is situated at a shallow depth in the northwest of Aluto below the Silti Debre Zeyt Fault Zone (SDFZ) as indicated by number 2 in the figure (Hübert et al., 2018). The magmatic and hydrothermal systems are connected through faults and fracture systems that extend deeper. Seismicity, magmatic intrusion below Aluto (indicated by number 1), rift and off-rift volcanoes are also illustrated.

in other volcanoes, such as Katla volcano under the Mýrdalsjökull glacier in South Iceland (Einarsson & Brandsdóttir, 2000). The abundant seismicity, elevated b-value, and high volatile phase content (Samrock et al., 2021) of the geothermal reservoir suggests it is critically stressed and sensitive to minor seasonal hydrological loading or stress changes. Our findings show that hydrological loading can induce seismicity, with seismic activity varying seasonally and could contribute to the source of unrest.

The high b-value at Aluto indicates the presence of fluids, and sampling CO_2 emissions from fumaroles have revealed a magmatic signature (Hutchison, Biggs, et al., 2016). This suggests repeated injections of magmatic fluids to shallow depths through preexisting faults and fracture systems. Both magmatic and hydrothermal processes could therefore be responsible for the unrest at Aluto. Differentiating between magmatic and hydrothermal processes based on deformation alone is not possible (Birhanu et al., 2018), although Hutchison, Biggs, et al. (2016) explain that edifice-wide inflation results from magmatic fluid injection and intrusion, followed by deflation due to magmatic degassing and hydrothermal system depressurization. Wilks, Kendall, et al. (2017); Wilks et al. (2020) attribute the source of deformation to deeper origins. According to Samrock et al. (2015), significant changes in the hydrothermal regime, specifically involving the hydro-mechanical behavior of clay minerals and thermoelastic expansion of fractured rock induced by hot fluids contribute to unrest.

Fault plane solutions for selected events reveal approximately NNE-SSW normal faults, consistent with the current direction of extension. These events, caused by brittle failure, display double-couple mechanisms, but fluids may also play a role in fault activation. The brittle nature of these events suggests that the NNE-SSW faults and the caldera ring faults are still active, potentially contributing to the unrest. Caldera ring faults can be reactivated during regional extension (Maestrelli et al., 2024). The NNE-SSW faults are located in the narrow zone of recent and intense faulting known as the WFB (Mohr, 1967). The structure and volcanic evolution of the Aluto volcanic complex are controlled by the influence of these NNE-trending faults (Le Turdu et al., 1999). All Quaternary volcanic activity has been limited to this belt, with no significant volcanic occurrences (Abebe et al., 1998) in the easternmost areas. The fault belt does not precisely align with the median axis of the rift and this deviation is attributed to a clockwise rotation rather than subsidence or uplift (Mohr, 1967). Geodetic data show that more than 80% of the strain within the rift is accommodated by magmatic segments, indicating that these faults are active and the border faults are not the primary areas of extension (Ebinger & Casey, 2001). The seismicity in these magmatic segments is of low magnitude and is prominent along Quaternary faults, fissures, and chains of eruptive centers (Keir et al., 2006).

The source of Aluto's unrest appears to involve a complex interplay of different mechanisms as deformation is influenced by various magmatic processes, including magma movement, crystallization, degassing and hydrothermal expansion (Caricchi et al., 2014; Kwoun et al., 2006; Mattia et al., 2007; Sigmundsson et al., 1997; Sturkell & Sigmundsson, 2000). Gas release can cause inflation unrelated to magma injection, and degassing or crystallization can lead to subsidence. At depths greater than 13 km mafic melts are saturated with H_2O and CO_2 and a considerable amount of volatiles are released from deep mafic melts through diffuse degassing (Iddon & Edmonds, 2020). These melts could be saturated with an exsolved volatile phase that has lower conductivity (Laumonier et al., 2017), but have high conductivity when mixed with groundwater (Aizawa et al., 2009), which might be observed at Aluto (Iddon & Edmonds, 2020). We suggest that the primary causes of unrest at Aluto are both magmatic and hydrothermal processes. These processes occur as faults and fracture systems channel fluids and intersect with shallow dikes or magma storage chambers. Additionally, the reactivation of caldera ring faults during regional extension and the impact of hydrological surface loading also play significant roles.

4.5. Wider Implications

Our observation of seismicity extending to greater depth beneath Aluto suggests a crystallized mush or body with melt pockets, which could have broader implications. Traditionally, melt-dominated magma chambers have been central to volcanic and igneous models. However, recent evidence challenges this view, suggesting that forming and maintaining such chambers is difficult. Geochemical studies reveal complex mineral scale processes and long-term near-solidus magma storage (Bachmann & Bergantz, 2008; Cashman et al., 2017; Cooper & Kent, 2014; Iddon et al., 2019). Large melt bodies are also frequently undetected by geophysical imaging beneath active volcanoes, suggesting magma may be stored as melt-poor mush with low conductivity and Vp/Vs ratio as mentioned above. An emerging consensus is that transcrustal magmatic systems are primarily composed of crystal mush, where crystals form a continuous framework interspersed with melt (Cashman et al., 2017; Jackson

et al., 2018; Sparks et al., 2019). This mush dominated perspective on igneous systems is highly explanatory, but it necessitates new conceptual models to address questions about magma evolution and volcanic system behavior. Shallow magma chambers either erupt as volcanoes or solidify as intrusive magma bodies (Cashman et al., 2017). Therefore, the intrusive body beneath Aluto is likely highly crystallized mush and could support the above argument. The parental melt originate from intricate, vertically extensive mafic magmatic systems located both on-axis and off-axis (Iddon & Edmonds, 2020). Additionally, the ascent of fluids along fault and fracture systems could have implications related to volcanic risk, shallow mineral deposits, and geothermal systems.

5. Conclusion

We analyzed the seismicity of Aluto and its surrounding region using a local network of 12 seismic stations operating from January 2012 to January 2014. A total of 2,393 events were located using a non-linear location method, with 1,262 events of sufficient quality to calculate moment magnitudes. The majority of the events beneath Aluto occur within the upper 2 km. Most of the events occur around the caldera and align with the NE-SW trending AJFZ, which cross-cuts the caldera edifice and ring faults. We observed temporal variations in seismicity. Seismic activity beneath Aluto extends up to 40 km bsl, and we observed low seismicity northwest of Aluto beneath SDFZ consistent with previous magnetotelluric and gravity studies. The high b-value suggest the presence of fluids and, pre-existing faults and fracture systems act as pathways connecting the magmatic system with the shallow hydrothermal system in Aluto. Fault plane solutions reveal approximately NNE-trending normal faults, consistent with the current direction of extension. Earthquakes are caused by brittle failure and display double-couple mechanisms, with fluids potentially playing a role in fault activation. The unrest at Aluto involves a complex interplay of different mechanisms, primarily driven by tectonic, magmatic and hydrothermal processes. The fluid pathways may control volcanic eruptions and facilitate mineral transport from a magmatic reservoir to the hydrothermal system, promoting mineral deposition at shallow depths.

Data Availability Statement

The XM seismic network and the waveforms that we used in this research are readily available for access and can be obtained through IRIS Data Services (The ARGOS Project, 2012). Earthquake locations are determined using QuakeMigrate (Bacon et al., 2025) and NonLinLoc (Lomax et al., 2023). The software used to calculate moment magnitudes and b-values, SeisSrcMoment (T. Hudson, 2020), is freely available. The algorithm used for moment tensor source inversion (Pugh & White, 2018) is also freely available. Several of the figures were created using Generic Mapping Tools (GMT) (Wessel et al., 2019), and the seismic data was analyzed using the ObsPy library (Beyreuther et al., 2010). The magnetotelluric (MT) model used in Figure 9 is available for download from the ETH research collection under Dambly et al. (2022), as a VTK file for visualization in ParaView. The event catalog generated in this study and borehole data are archived and available through Zenodo (Yemane et al., 2025).

Acknowledgments

We express our gratitude to SEIS-UK for generously providing their seismic equipment under GEF loan 962 and for their valuable assistance. Additionally, we extend our thanks to the collaborators at the Ethiopian Electric Power Corporation (EEPCo) and the Geological Survey of Ethiopia (GSE) for their significant contributions to the project. The Bristol University Microseismic Projects (BUMPS) played a crucial role by funding the seismic experiment and fieldwork. The authors would like to acknowledge the use of the University of Oxford Advanced Research Computing (ARC) facility in carrying out this work. http://dx.doi.org/10.5281/zenodo.22558. TY is supported by a Clarendon Scholarship from the University of Oxford.

References

Abebe, T., Mazzarini, F., Innocenti, F., & Manetti, P. (1998). The Yerer-Tullu Wellel volcanotectonic lineament: A transtensional structure in central Ethiopia and the associated magmatic activity. *Journal of African Earth Sciences*, *26*(1), 135–150. https://doi.org/10.1016/s0899-5362(97)00141-3

Acocella, V., Di Lorenzo, R., Newhall, C., & Scandone, R. (2015). An overview of recent (1988 to 2014) caldera unrest: Knowledge and perspectives. *Reviews of Geophysics*, *53*(3), 896–955. https://doi.org/10.1002/2015rg000492

Agostini, A., Marco, B., Giacomo, C., Federico, S., & Francesco, M. (2011). Fault architecture in the Main Ethiopian Rift and comparison with experimental models: Implications for rift evolution and Nubia–Somalia kinematics. *Earth and Planetary Science Letters*, *301*(3–4), 479–492. https://doi.org/10.1016/j.epsl.2010.11.024

Agostini, A., Marco, B., Giacomo, C., Federico, S., & Piero, M. (2011). Distribution of quaternary deformation in the central Main Ethiopian Rift, East Africa. *Tectonics*, *30*(4). https://doi.org/10.1029/2010tc002833

Aizawa, K., Ogawa, Y., & Ishido, T. (2009). Groundwater flow and hydrothermal systems within volcanic edifices: Delineation by electric self-potential and magnetotellurics. *Journal of Geophysical Research*, *114*(B1). https://doi.org/10.1029/2008jb005910

Albaric, J., Deverchere, J., Perrot, J., Jakovlev, A., & Deschamps, A. (2014). Deep crustal earthquakes in North Tanzania, East Africa: Interplay between tectonic and magmatic processes in an incipient rift. *Geochemistry, Geophysics, Geosystems*, *15*(2), 374–394. https://doi.org/10.1002/2013gc005027

Albino, F., & Biggs, J. (2021). Magmatic processes in the East African Rift System: Insights from a 2015–2020 Sentinel-1 InSAR survey. *Geochemistry, Geophysics, Geosystems*, *22*(3), e2020GC009488. https://doi.org/10.1029/2020gc009488

Ayele, A. (2000). Normal left-oblique fault mechanisms as an indication of sinistral deformation between the Nubia and Somalia plates in the Main Ethiopian Rift. *Journal of African Earth Sciences*, *31*(2), 359–367. https://doi.org/10.1016/s0899-5362(00)00093-2

Bachmann, O., & Bergantz, G. (2008). The magma reservoirs that feed supereruptions. *Elements*, *4*(1), 17–21. https://doi.org/10.2113/gselements.4.1.17

Bachmann, O., Wiemer, S., Goertz-Allmann, B., & Woessner, J. (2012). Influence of pore-pressure on the event-size distribution of induced earthquakes. *Geophysical Research Letters*, *39*(9). https://doi.org/10.1029/2012gl051480

Bacon, C., Winder, T., Greenfield, T., & Bot, S. (2025). QuakeMigrate v1.2.0 [Software]. *Zenodo*. https://doi.org/10.5281/zenodo.15185641

Bastow, I., Pilidou, S., Kendall, J.-M., & Stuart, G. (2010). Melt-induced seismic anisotropy and magma assisted rifting in Ethiopia: Evidence from surface waves. *Geochemistry, Geophysics, Geosystems*, *11*(6). https://doi.org/10.1029/2010gc003036

Benti, N. E., Woldegiyorgis, T. A., Geffe, C. A., Gurmesa, G. S., Chaka, M. D., & Mekonnen, Y. S. (2023). Overview of geothermal resources utilization in Ethiopia: Potentials, opportunities, and challenges. *Scientific African*, *19*, e01562. https://doi.org/10.1016/j.sciaf.2023.e01562

Beyreuther, M., Barsch, R., Krischer, L., Megies, T., Behr, Y., & Wassermann, J. (2010). ObsPy: A Python toolbox for seismology. *Seismological Research Letters*, *81*(3), 530–533. https://doi.org/10.1785/gssrl.81.3.530

Biggs, J., Bastow, I., Keir, D., & Lewi, E. (2011). Pulses of deformation reveal frequently recurring shallow magmatic activity beneath the Main Ethiopian Rift. *Geochemistry, Geophysics, Geosystems*, *12*(9). https://doi.org/10.1029/2011gc003662

Bilham, R., Bendick, R., Larson, K., Mohr, P., Braun, J., Tesfaye, S., & Asfaw, L. (1999). Secular and tidal strain across the Main Ethiopian Rift. *Geophysical Research Letters*, *26*(18), 2789–2792. https://doi.org/10.1029/1998gl005315

Birhanu, Y., Wilks, M., Biggs, J., Kendall, J.-M., Ayele, A., & Lewi, E. (2018). Seasonal patterns of seismicity and deformation at the Alutu geothermal reservoir, Ethiopia, induced by hydrological loading. *Journal of Volcanology and Geothermal Research*, *356*, 175–182. https://doi.org/10.1016/j.jvolgeores.2018.03.008

Blundy, J., Afanasyev, A., Tattitch, B., Sparks, S., Melnik, O., Utkin, I., & Rust, A. (2021). The economic potential of metalliferous sub-volcanic brines. *Royal Society Open Science*, *8*(6), 202192. https://doi.org/10.1098/rsos.202192

Boccaletti, M., Bonini, M., Mazzuoli, R., Abebe, B., Piccardi, L., & Tortorici, L. (1998). Quaternary oblique extensional tectonics in the Ethiopian Rift (Horn of Africa). *Tectonophysics*, *287*(1–4), 97–116. https://doi.org/10.1016/s0040-1951(98)80063-2

Boccaletti, M., Mazzuoli, R., Bonini, M., Trua, T., & Abebe, B. (1999). Plio-Quaternary volcanotectonic activity in the northern sector of the Main Ethiopian Rift: Relationships with oblique rifting. *Journal of African Earth Sciences*, *29*(4), 679–698. https://doi.org/10.1016/s0899-5362(99)00124-4

Bonini, M., Corti, G., Innocenti, F., Manetti, P., Mazzarini, F., Abebe, T., & Pecskay, Z. (2005). Evolution of the Main Ethiopian Rift in the frame of Afar and Kenya rifts propagation. *Tectonics*, *24*(1). https://doi.org/10.1029/2004tc001680

Bonini, M., Souriot, T., Boccaletti, M., & Brun, J. P. (1997). Successive orthogonal and oblique extension episodes in a rift zone: Laboratory experiments with application to the Ethiopian rift. *Tectonics*, *16*(2), 347–362. https://doi.org/10.1029/96tc03935

Bridges, D. L., & Gao, S. S. (2006). Spatial variation of seismic b-values beneath Makushin Volcano, Unalaska Island, Alaska. *Earth and Planetary Science Letters*, *245*(1–2), 408–415. https://doi.org/10.1016/j.epsl.2006.03.010

Brune, J. N. (1970). Tectonic stress and the spectra of seismic shear waves from earthquakes. *Journal of Geophysical Research*, *75*(26), 4997–5009. https://doi.org/10.1029/jb075i026p04997

Calais, E., Ebinger, C., Hartnady, C., & Nocquet, J. (2006). Kinematics of the East African Rift from GPS and earthquake slip vector data. *Geological Society, London, Special Publications*, *259*(1), 9–22. https://doi.org/10.1144/gsl.sp.2006.259.01.03

Caricchi, L., Biggs, J., Annen, C., & Ebmeier, S. (2014). The influence of cooling, crystallisation and re-melting on the interpretation of geodetic signals in volcanic systems. *Earth and Planetary Science Letters*, *388*, 166–174. https://doi.org/10.1016/j.epsl.2013.12.002

Cashman, K. V., Sparks, R. S. J., & Blundy, J. D. (2017). Vertically extensive and unstable magmatic systems: A unified view of igneous processes. *Science*, *355*(6331), eaag3055. https://doi.org/10.1126/science.aag3055

Chambers, E. L., Harmon, N., Rychert, C. A., & Keir, D. (2021). Variations in melt emplacement beneath the northern East African Rift from radial anisotropy. *Earth and Planetary Science Letters*, *573*, 117150. https://doi.org/10.1016/j.epsl.2021.117150

Chapman, C., & Leaney, W. (2012). A new moment-tensor decomposition for seismic events in anisotropic media. *Geophysical Journal International*, *188*(1), 343–370. https://doi.org/10.1111/j.1365-246x.2011.05265.x

Chen, W.-P., & Molnar, P. (1983). Focal depths of intracontinental and intraplate earthquakes and their implications for the thermal and mechanical properties of the lithosphere. *Journal of Geophysical Research*, *88*(B5), 4183–4214. https://doi.org/10.1029/jb088ib05p04183

Cherkose, B. A., & Mizunaga, H. (2018). Resistivity imaging of Aluto-Langano geothermal field using 3-D magnetotelluric inversion. *Journal of African Earth Sciences*, *139*, 307–318. https://doi.org/10.1016/j.jafrearsci.2017.12.017

Cooper, K. M., & Kent, A. J. (2014). Rapid remobilization of magmatic crystals kept in cold storage. *Nature*, *506*(7489), 480–483. https://doi.org/10.1038/nature12991

Cornwell, D., Mackenzie, G., England, R., Maguire, P., Asfaw, L., & Oluma, B. (2006). Northern Main Ethiopian Rift crustal structure from new high-precision gravity data. *Geological Society, London, Special Publications*, *259*(1), 307–321. https://doi.org/10.1144/gsl.sp.2006.259.01.23

Corti, G. (2008). Control of rift obliquity on the evolution and segmentation of the main Ethiopian Rift. *Nature Geoscience*, *1*(4), 258–262. https://doi.org/10.1038/ngeo160

Corti, G. (2009). Continental rift evolution: From rift initiation to incipient break-up in the Main Ethiopian Rift, East Africa. *Earth-Science Reviews*, *96*(1–2), 1–53. https://doi.org/10.1016/j.earscirev.2009.06.005

Corti, G., Bonini, M., Conticelli, S., Innocenti, F., Manetti, P., & Sokoutis, D. (2003). Analogue modelling of continental extension: A review focused on the relations between the patterns of deformation and the presence of magma. *Earth-Science Reviews*, *63*(3–4), 169–247. https://doi.org/10.1016/s0012-8252(03)00035-7

Daly, E., Keir, D., Ebinger, C., Stuart, G., Bastow, I., & Ayele, A. (2008). Crustal tomographic imaging of a transitional continental rift: The Ethiopian Rift. *Geophysical Journal International*, *172*(3), 1033–1048. https://doi.org/10.1111/j.1365-246x.2007.03682.x

Dambly, M., Samrock, F., Grayver, A., & Saar, M. O. (2023). Insights on the interplay of rifting, transcrustal magmatism and formation of geothermal resources in the central segment of the Ethiopian Rift revealed by 3-d magnetotelluric imaging. *Journal of Geophysical Research: Solid Earth*, *128*(7), e2022JB025849. https://doi.org/10.1029/2022jb025849

Dambly, M., Samrock, F., Grayver, A., & Saar, M. O. (2022). Transcrustal 3-D electrical conductivity model of the Central Main Ethiopian Rift [Dataset]. *ETH Research Collection*. https://doi.org/10.3929/ethz-b-000576313

De Gori, P., Lucente, F. P., Lombardi, A. M., Chiarabba, C., & Montuori, C. (2012). Heterogeneities along the 2009 L'Aquila normal fault inferred by the b-value distribution. *Geophysical Research Letters*, *39*(15). https://doi.org/10.1029/2012gl052822

Deichmann, N. (2006). Local magnitude, a moment revisited. *Bulletin of the Seismological Society of America*, *96*(4A), 1267–1277. https://doi.org/10.1785/0120050115

Déverchère, J., Petit, C., Gileva, N., Radziminovitch, N., Melnikova, V., & San'Kov, V. (2001). Depth distribution of earthquakes in the Baikal rift system and its implications for the rheology of the lithosphere. *Geophysical Journal International*, *146*(3), 714–730. https://doi.org/10.1046/j.0956-540x.2001.1484.484.x

Drew, J., White, R. S., Tilmann, F., & Tarasewicz, J. (2013). Coalescence microseismic mapping. *Geophysical Journal International*, *195*(3), 1773–1785. https://doi.org/10.1093/gji/ggt331

Ebinger, C., & Casey, M. (2001). Continental breakup in magmatic provinces: An Ethiopian example. *Geology*, *29*(6), 527–530. https://doi.org/10.1130/0091-7613(2001)029<0527:cbimpa>2.0.co;2

Einarsson, P., & Brandsdóttir, B. (2000). Earthquakes in the Mỳrdalsjökull area, Iceland, 1978–1985: Seasonal correlation and connection with volcanoes. *Jökull Journal*, *49*, 59–73.

El-Isa, Z. H., & Eaton, D. W. (2014). Spatiotemporal variations in the b-value of earthquake magnitude–frequency distributions: Classification and causes. *Tectonophysics*, *615*, 1–11. https://doi.org/10.1016/j.tecto.2013.12.001

Fontijn, K., McNamara, K., Tadesse, A. Z., Pyle, D. M., Dessalegn, F., Hutchison, W., et al. (2018). Contrasting styles of post-caldera volcanism along the Main Ethiopian Rift: Implications for contemporary volcanic hazards. *Journal of Volcanology and Geothermal Research*, *356*, 90–113. https://doi.org/10.1016/j.jvolgeores.2018.02.001

Frohlich, C., & Davis, S. D. (1993). Teleseismic b values; Or, much ado about 1.0. *Journal of Geophysical Research*, *98*(B1), 631–644. https://doi.org/10.1029/92jb01891

Gauntlett, M., Hudson, T., Kendall, J.-M., Rawlinson, N., Blundy, J., Lapins, S., et al. (2023). Seismic tomography of Nabro caldera, Eritrea: Insights into the magmatic and hydrothermal systems of a recently erupted volcano. *Journal of Geophysical Research: Solid Earth*, *128*(5), e2022JB025742. https://doi.org/10.1029/2022jb025742

Gianelli, G., & Teklemariam, M. (1993). Water-rock interaction processes in the Aluto-Langano geothermal field (Ethiopia). *Journal of Volcanology and Geothermal Research*, *56*(4), 429–445. https://doi.org/10.1016/0377-0273(93)90007-e

Gizaw, B. (1993). Aluto-Langano geothermal field, Ethiopian Rift Valley: Physical characteristics and the effects of gas on well performance. *Geothermics*, *22*(2), 101–116. https://doi.org/10.1016/0375-6505(93)90050-w

Gleeson, M. L., Stock, M. J., Pyle, D. M., Mather, T. A., Hutchison, W., Yirgu, G., & Wade, J. (2017). Constraining magma storage conditions at a restless volcano in the Main Ethiopian Rift using phase equilibria models. *Journal of Volcanology and Geothermal Research*, *337*, 44–61. https://doi.org/10.1016/j.jvolgeores.2017.02.026

Greenfield, T., Keir, D., Kendall, J.-M., & Ayele, A. (2019a). Low-frequency earthquakes beneath Tullu Moye volcano, Ethiopia, reveal fluid pulses from shallow magma chamber. *Earth and Planetary Science Letters*, *526*, 115782. https://doi.org/10.1016/j.epsl.2019.115782

Greenfield, T., Keir, D., Kendall, J.-M., & Ayele, A. (2019b). Seismicity of the Bora-Tullu Moye volcanic field, 2016–2017. *Geochemistry, Geophysics, Geosystems*, *20*(2), 548–570. https://doi.org/10.1029/2018gc007648

Greenfield, T., & White, R. S. (2015). Building Icelandic igneous crust by repeated melt injections. *Journal of Geophysical Research: Solid Earth*, *120*(11), 7771–7788. https://doi.org/10.1002/2015jb012009

Greenfield, T., White, R. S., Winder, T., & Ágústsdóttir, T. (2020). Seismicity of the Askja and Bárdharbunga volcanic systems of Iceland, 2009–2015. *Journal of Volcanology and Geothermal Research*, *391*, 106432. https://doi.org/10.1016/j.jvolgeores.2018.08.010

Gresse, M., Uyeshima, M., Koyama, T., Hase, H., Aizawa, K., Yamaya, Y., et al. (2021). Hydrothermal and magmatic system of a volcanic island inferred from magnetotellurics, seismicity, self-potential, and thermal image: An example of Miyakejima (Japan). *Journal of Geophysical Research: Solid Earth*, *126*(6), e2021JB022034. https://doi.org/10.1029/2021jb022034

Gutenberg, B., & Richter, C. F. (1944). Frequency of earthquakes in California. *Bulletin of the Seismological Society of America*, *34*(4), 185–188. https://doi.org/10.1785/bssa0340040185

Hammond, J. O., Kendall, J.-M., Wookey, J., Stuart, G., Keir, D., & Ayele, A. (2014). Differentiating flow, melt, or fossil seismic anisotropy beneath Ethiopia. *Geochemistry, Geophysics, Geosystems*, *15*(5), 1878–1894. https://doi.org/10.1002/2013gc005185

Hardebeck, J. L., & Shearer, P. M. (2002). A new method for determining first-motion focal mechanisms. *Bulletin of the Seismological Society of America*, *92*(6), 2264–2276. https://doi.org/10.1785/0120010200

Hardebeck, J. L., & Shearer, P. M. (2003). Using S/P amplitude ratios to constrain the focal mechanisms of small earthquakes. *Bulletin of the Seismological Society of America*, *93*(6), 2434–2444. https://doi.org/10.1785/0120020236

Hedenquist, J. W., & Lowenstern, J. B. (1994). The role of magmas in the formation of hydrothermal ore deposits. *Nature*, *370*(6490), 519–527. https://doi.org/10.1038/370519a0

Heřmanská, M., Stefánsson, A., & Scott, S. (2019). Supercritical fluids around magmatic intrusions: IDDP-1 at Krafla, Iceland. *Geothermics*, *78*, 101–110. https://doi.org/10.1016/j.geothermics.2018.11.002

Herrmann, M., Piegari, E., & Marzocchi, W. (2022). Revealing the spatiotemporal complexity of the magnitude distribution and b-value during an earthquake sequence. *Nature Communications*, *13*(1), 5087. https://doi.org/10.1038/s41467-022-32755-6

Hochstein, M. P., Oluma, B., & Hole, H. (2017). Early exploration of the Aluto geothermal field, Ethiopia (History of discovery well LA-3). *Geothermics*, *66*, 73–84. https://doi.org/10.1016/j.geothermics.2016.11.010

Hübert, J., Whaler, K., & Fisseha, S. (2018). The electrical structure of the central Main Ethiopian Rift as imaged by magnetotellurics: Implications for magma storage and pathways. *Journal of Geophysical Research: Solid Earth*, *123*(7), 6019–6032. https://doi.org/10.1029/2017jb015160

Hudson, J., Pearce, R., & Rogers, R. (1989). Source type plot for inversion of the moment tensor. *Journal of Geophysical Research*, *94*(B1), 765–774. https://doi.org/10.1029/jb094ib01p00765

Hudson, T. (2020). SeisSrcMoment: First formal release (1.0.0) [Software]. *Zenodo*. https://doi.org/10.5281/zenodo.4010325

Hudson, T., Kendall, J.-M., Blundy, J. D., Pritchard, M. E., MacQueen, P., Wei, S., et al. (2023). Hydrothermal fluids and where to find them: Using seismic attenuation and anisotropy to map fluids beneath Uturuncu volcano, Bolivia. *Geophysical Research Letters*, *50*(5), e2022GL100974. https://doi.org/10.1029/2022gl100974

Hudson, T., Kendall, J.-M., Pritchard, M. E., Blundy, J. D., & Gottsmann, J. H. (2022). From slab to surface: Earthquake evidence for fluid migration at Uturuncu volcano, Bolivia. *Earth and Planetary Science Letters*, *577*, 117268. https://doi.org/10.1016/j.epsl.2021.117268

Hudson, T., Smith, J., Brisbourne, A. M., & White, R. S. (2019). Automated detection of basal icequakes and discrimination from surface crevassing. *Annals of Glaciology*, *60*(79), 167–181. https://doi.org/10.1017/aog.2019.18

Hudson, T., White, R., Greenfield, T., Agustsdottir, T., Brisbourne, A., & Green, R. (2017). Deep crustal melt plumbing of Bárdharbunga volcano, Iceland. *Geophysical Research Letters*, *44*(17), 8785–8794. https://doi.org/10.1002/2017gl074749

Hunt, J. A., Mather, T. A., & Pyle, D. M. (2020). Morphological comparison of distributed volcanic fields in the Main Ethiopian Rift using high-resolution digital elevation models. *Journal of Volcanology and Geothermal Research*, *393*, 106732. https://doi.org/10.1016/j.jvolgeores.2019.106732

Hunt, J. A., Zafu, A., Mather, T. A., Pyle, D. M., & Barry, P. H. (2017). Spatially variable CO_2 degassing in the Main Ethiopian Rift: Implications for magma storage, volatile transport, and rift-related emissions. *Geochemistry, Geophysics, Geosystems*, *18*(10), 3714–3737. https://doi.org/10.1002/2017gc006975

Hutchison, W., Biggs, J., Mather, T. A., Pyle, D. M., Lewi, E., Yirgu, G., et al. (2016). Causes of unrest at silicic calderas in the East African Rift: New constraints from InSAR and soil-gas chemistry at Aluto volcano, Ethiopia. *Geochemistry, Geophysics, Geosystems*, *17*(8), 3008–3030. https://doi.org/10.1002/2016gc006395

Hutchison, W., Fusillo, R., Pyle, D. M., Mather, T. A., Blundy, J. D., Biggs, J., et al. (2016). A pulse of mid-pleistocene rift volcanism in Ethiopia at the dawn of modern humans. *Nature Communications*, *7*(1), 13192. https://doi.org/10.1038/ncomms13192

Hutchison, W., Mather, T. A., Pyle, D. M., Biggs, J., & Yirgu, G. (2015). Structural controls on fluid pathways in an active Rift System: A case study of the Aluto volcanic complex. *Geosphere*, *11*(3), 542–562. https://doi.org/10.1130/ges01119.1

Hutchison, W., Mather, T. A., Pyle, D. M., Boyce, A. J., Gleeson, M. L., Yirgu, G., et al. (2018). The evolution of magma during continental rifting: New constraints from the isotopic and trace element signatures of silicic magmas from Ethiopian volcanoes. *Earth and Planetary Science Letters*, *489*, 203–218. https://doi.org/10.1016/j.epsl.2018.02.027

Hutchison, W., Pyle, D. M., Mather, T. A., Yirgu, G., Biggs, J., Cohen, B. E., et al. (2016). The eruptive history and magmatic evolution of Aluto volcano: New insights into silicic peralkaline volcanism in the Ethiopian rift. *Journal of Volcanology and Geothermal Research*, *328*, 9–33. https://doi.org/10.1016/j.jvolgeores.2016.09.010

Iddon, F., & Edmonds, M. (2020). Volatile-rich magmas distributed through the upper crust in the Main Ethiopian Rift. *Geochemistry, Geophysics, Geosystems*, *21*(6), e2019GC008904. https://doi.org/10.1029/2019gc008904

Iddon, F., Jackson, C., Hutchison, W., Fontijn, K., Pyle, D. M., Mather, T. A., et al. (2019). Mixing and crystal scavenging in the Main Ethiopian Rift revealed by trace element systematics in feldspars and glasses. *Geochemistry, Geophysics, Geosystems*, *20*(1), 230–259. https://doi.org/10.1029/2018gc007836

Jackson, M., Blundy, J., & Sparks, R. (2018). Chemical differentiation, cold storage and remobilization of magma in the earth's crust. *Nature*, *564*(7736), 405–409. https://doi.org/10.1038/s41586-018-0746-2

Jolie, E., Hutchison, W., Driba, D. L., Jentsch, A., & Gizaw, B. (2019). Pinpointing deep geothermal upflow in zones of complex tectono-volcanic degassing: New insights from Aluto volcano, Main Ethiopian Rift. *Geochemistry, Geophysics, Geosystems*, *20*(8), 4146–4161. https://doi.org/10.1029/2019gc008309

Jolie, E., Scott, S., Faulds, J., Chambefort, I., Axelsson, G., Gutiérrez-Negrín, L. C., et al. (2021). Geological controls on geothermal resources for power generation. *Nature Reviews Earth & Environment*, *2*(5), 324–339. https://doi.org/10.1038/s43017-021-00154-y

Kanamori, H. (1977). The energy release in great earthquakes. *Journal of Geophysical Research*, *82*(20), 2981–2987. https://doi.org/10.1029/jb082i020p02981

Kebede, B. A., Pagli, C., Sigmundsson, F., Keir, D., La Rosa, A., & Guðbrandsson, S. (2023). Constraints on ground deformation processes at the Tulu Moye volcanic complex, Main Ethiopian Rift. *Journal of Volcanology and Geothermal Research*, *438*, 107810. https://doi.org/10.1016/j.jvolgeores.2023.107810

Keir, D., Bastow, I. D., Corti, G., Mazzarini, F., & Rooney, T. O. (2015). The origin of along-rift variations in faulting and magmatism in the Ethiopian Rift. *Tectonics*, *34*(3), 464–477. https://doi.org/10.1002/2014tc003698

Keir, D., Bastow, I. D., Whaler, K. A., Daly, E., Cornwell, D. G., & Hautot, S. (2009). Lower crustal earthquakes near the Ethiopian rift induced by magmatic processes. *Geochemistry, Geophysics, Geosystems*, *10*(6). https://doi.org/10.1029/2009gc002382

Keir, D., Belachew, M., Ebinger, C., Kendall, J.-M., Hammond, J. O., Stuart, G., et al. (2011). Mapping the evolving strain field during continental breakup from crustal anisotropy in the Afar Depression. *Nature Communications*, *2*(1), 285. https://doi.org/10.1038/ncomms1287

Keir, D., Ebinger, C., Stuart, G., Daly, E., & Ayele, A. (2006). Strain accommodation by magmatism and faulting as rifting proceeds to breakup: Seismicity of the northern Ethiopian rift. *Journal of Geophysical Research*, *111*(B5). https://doi.org/10.1029/2005jb003748

Kendall, J.-M., Pilidou, S., Keir, D., Bastow, I., Stuart, G., & Ayele, A. (2006). Mantle upwellings, melt migration and the rifting of Africa: Insights from seismic anisotropy. *Geological Society, London, Special Publications*, *259*(1), 55–72. https://doi.org/10.1144/gsl.sp.2006.259.01.06

Kendall, J.-M., Stuart, G., Ebinger, C., Bastow, I. D., & Keir, D. (2005). Magma-assisted rifting in Ethiopia. *Nature*, *433*(7022), 146–148. https://doi.org/10.1038/nature03161

Keranen, K., Klemperer, S., Gloaguen, R., & Group, E. W. (2004). Three-dimensional seismic imaging of a protoridge axis in the Main Ethiopian Rift. *Geology*, *32*(11), 949–952. https://doi.org/10.1130/g20737.1

Kwoun, O.-I., Lu, Z., Neal, C., & Wicks, C. (2006). Quiescent deformation of the Aniakchak Caldera, Alaska, mapped by InSAR. *Geology*, *34*(1), 5–8. https://doi.org/10.1130/g22015.1

Lapins, S., Kendall, J. M., Ayele, A., Wilks, M., Nowacki, A., & Cashman, K. V. (2020). Lower-crustal seismicity on the eastern border faults of the Main Ethiopian Rift. *Journal of Geophysical Research: Solid Earth*, *125*(8), e2020JB020030. https://doi.org/10.1029/2020jb020030

Laumonier, M., Gaillard, F., Muir, D., Blundy, J., & Unsworth, M. (2017). Giant magmatic water reservoirs at mid-crustal depth inferred from electrical conductivity and the growth of the continental crust. *Earth and Planetary Science Letters*, *457*, 173–180. https://doi.org/10.1016/j.epsl.2016.10.023

Lavayssière, A., Drooff, C., Ebinger, C., Gallacher, R., Illsley-Kemp, F., Oliva, S. J., & Keir, D. (2019). Depth extent and kinematics of faulting in the southern Tanganyika Rift, Africa. *Tectonics*, *38*(3), 842–862. https://doi.org/10.1029/2018tc005379

Lavayssière, A., Greenfield, T., Keir, D., Ayele, A., & Kendall, J.-M. (2019). Local seismicity near the actively deforming Corbetti volcano in the Main Ethiopian Rift. *Journal of Volcanology and Geothermal Research*, *381*, 227–237. https://doi.org/10.1016/j.jvolgeores.2019.06.008

Le Turdu, C., Tiercelin, J.-J., Gibert, E., Travi, Y., Lezzar, K.-E., Richert, J.-P., et al. (1999). The Ziway–Shala lake basin system, Main Ethiopian Rift: Influence of volcanism, tectonics, and climatic forcing on basin formation and sedimentation. *Palaeogeography, Palaeoclimatology, Palaeoecology*, *150*(3–4), 135–177. https://doi.org/10.1016/s0031-0182(98)00220-x

Lindenfeld, M., & Rümpker, G. (2011). Detection of mantle earthquakes beneath the East African Rift. *Geophysical Journal International*, *186*(1), 1–5. https://doi.org/10.1111/j.1365-246x.2011.05048.x

Lloyd, R., Biggs, J., Wilks, M., Nowacki, A., Kendall, J.-M., Ayele, A., et al. (2018). Evidence for cross rift structural controls on deformation and seismicity at a continental rift caldera. *Earth and Planetary Science Letters*, *487*, 190–200. https://doi.org/10.1016/j.epsl.2018.01.037

Lomax, A. (2005). A reanalysis of the hypocentral location and related observations for the great 1906 California earthquake. *Bulletin of the Seismological Society of America*, *95*(3), 861–877. https://doi.org/10.1785/0120040141

Lomax, A., & Curtis, A. (2001). Fast, probabilistic earthquake location in 3D models using oct-tree importance sampling. *Geophysical Research Abstracts*, *3*, 10–1007.

Lomax, A., Megies, T., Ho, S., Saurel, J.-M., & Luca, S. (2023). NonLinLoc: Intermittent release to enable citing and reference of NonLinLoc through Zenodo (v7.00.16-beta) [Software]. *Zenodo*. https://doi.org/10.5281/zenodo.8046170

Lomax, A., Virieux, J., Volant, P., & Berge-Thierry, C. (2000). Probabilistic earthquake location in 3D and layered models: Introduction of a Metropolis-Gibbs method and comparison with linear locations. *Advances in Seismic Event Location*, 101–134.

Mackenzie, G., Thybo, H., & Maguire, P. (2005). Crustal velocity structure across the Main Ethiopian Rift: Results from two-dimensional wide-angle seismic modelling. *Geophysical Journal International*, *162*(3), 994–1006. https://doi.org/10.1111/j.1365-246x.2005.02710.x

Maestrelli, D., Corti, G., Bonini, M., Keir, D., Facincani, P., Vannucchi, P., et al. (2024). Fault reactivation and growth at rift-related calderas. *Earth and Planetary Science Letters*, *636*, 118700. https://doi.org/10.1016/j.epsl.2024.118700

Maguire, P., Keller, G., Klemperer, S., Mackenzie, G., Keranen, K., Harder, S., et al. (2006). Crustal structure of the northern Main Ethiopian Rift from the EAGLE controlled-source survey; a snapshot of incipient lithospheric break-up. *Geological Society, London, Special Publications*, *259*(1), 269–292. https://doi.org/10.1144/gsl.sp.2006.259.01.21

Manley, G. F., Mather, T. A., Pyle, D. M., Clifton, D. A., Rodgers, M., Thompson, G., & Roman, D. C. (2021). Machine learning approaches to identifying changes in eruptive state using multi-parameter datasets from the 2006 eruption of Augustine volcano, Alaska. *Journal of Geophysical Research: Solid Earth*, *126*(12), e2021JB022323. https://doi.org/10.1029/2021jb022323

Mattia, M., Bonaccorso, A., & Guglielmino, F. (2007). Ground deformations in the Island of Pantelleria (Italy): Insights into the dynamic of the current intereruptive period. *Journal of Geophysical Research*, *112*(B11). https://doi.org/10.1029/2006jb004781

Mazzarini, F., Keir, D., & Isola, I. (2013). Spatial relationship between earthquakes and volcanic vents in the central-northern Main Ethiopian Rift. *Journal of Volcanology and Geothermal Research*, *262*, 123–133. https://doi.org/10.1016/j.jvolgeores.2013.05.007

McNamara, K., Cashman, K., Rust, A., Fontijn, K., Chalié, F., Tomlinson, E. L., & Yirgu, G. (2018). Using lake sediment cores to improve records of volcanism at Aluto volcano in the Main Ethiopian Rift. *Geochemistry, Geophysics, Geosystems*, *19*(9), 3164–3188. https://doi.org/10.1029/2018gc007686

McNutt, S. R. (2005). Volcanic seismology. *Annual Review of Earth and Planetary Sciences*, *32*(1), 461–491. https://doi.org/10.1146/annurev.earth.33.092203.122459

Mickus, K., Tadesse, K., Keller, G., & Oluma, B. (2007). Gravity analysis of the Main Ethiopian Rift. *Journal of African Earth Sciences*, *48*(2–3), 59–69. https://doi.org/10.1016/j.jafrearsci.2007.02.008

Mohr, P. (1967). Major volcano–tectonic lineament in the Ethiopian Rift system. *Nature*, *213*(5077), 664–665. https://doi.org/10.1038/213664a0

Moser, T., Van Eck, T., & Nolet, G. (1992). Hypocenter determination in strongly heterogeneous earth models using the shortest path method. *Journal of Geophysical Research*, *97*(B5), 6563–6572. https://doi.org/10.1029/91jb03176

Mulugeta, B. D., Fujimitsu, Y., Nishijima, J., & Saibi, H. (2021). Interpretation of gravity data to delineate the subsurface structures and reservoir geometry of the Aluto–Langano geothermal field, Ethiopia. *Geothermics*, *94*, 102093. https://doi.org/10.1016/j.geothermics.2021.102093

Nigussie, W., Alemu, A., Muluneh, A. A., Mickus, K., Muhabaw, Y., & Ballay, M. (2023). Formation of magmatic segments within the Aluto-Gedemsa area, Main Ethiopian Rift. *Italian Journal of Geosciences*, *142*(1), 28–41. https://doi.org/10.3301/ijg.2023.02

Nowacki, A., Wilks, M., Kendall, J.-M., Biggs, J., & Ayele, A. (2018). Characterising hydrothermal fluid pathways beneath Aluto volcano, Main Ethiopian Rift, using shear wave splitting. *Journal of Volcanology and Geothermal Research*, *356*, 331–341. https://doi.org/10.1016/j.jvolgeores.2018.03.023

Nyblade, A. A., & Langston, C. A. (1995). East African earthquakes below 20 km depth and their implications for crustal structure. *Geophysical Journal International*, *121*(1), 49–62. https://doi.org/10.1111/j.1365-246x.1995.tb03510.x

Okamoto, K., Asanuma, H., Ishibashi, T., Yamaya, Y., Saishu, H., Yanagisawa, N., et al. (2019). Geological and engineering features of developing ultra-high-temperature geothermal systems in the world. *Geothermics*, *82*, 267–281. https://doi.org/10.1016/j.geothermics.2019.07.002

Ottemoller, L., & Havskov, J. (2003). Moment magnitude determination for local and regional earthquakes based on source spectra. *Bulletin of the Seismological Society of America*, *93*(1), 203–214. https://doi.org/10.1785/0120010220

Peccerillo, A., Donati, C., Santo, A., Orlando, A., Yirgu, G., & Ayalew, D. (2007). Petrogenesis of silicic peralkaline rocks in the Ethiopian Rift: Geochemical evidence and volcanological implications. *Journal of African Earth Sciences*, *48*(2–3), 161–173. https://doi.org/10.1016/j.jafrearsci.2006.06.010

Petruccelli, A., Schorlemmer, D., Tormann, T., Rinaldi, A. P., Wiemer, S., Gasperini, P., & Vannucci, G. (2019). The influence of faulting style on the size-distribution of global earthquakes. *Earth and Planetary Science Letters*, *527*, 115791. https://doi.org/10.1016/j.epsl.2019.115791

Podvin, P., & Lecomte, I. (1991). Finite difference computation of traveltimes in very contrasted velocity models: A massively parallel approach and its associated tools. *Geophysical Journal International*, *105*(1), 271–284. https://doi.org/10.1111/j.1365-246x.1991.tb03461.x

Pritchard, M., Mather, T., McNutt, S. R., Delgado, F., & Reath, K. (2019). Thoughts on the criteria to determine the origin of volcanic unrest as magmatic or non-magmatic. *Philosophical Transactions of the Royal Society A*, *377*(2139), 20180008. https://doi.org/10.1098/rsta.2018.0008

Pugh, D., & White, R. (2018). Mtfit: A Bayesian approach to seismic moment tensor inversion. *Seismological Research Letters*, *89*(4), 1507–1513. https://doi.org/10.17863/CAM.25594

Pugh, D., White, R., & Christie, P. (2016). A Bayesian method for microseismic source inversion. *Geophysical Journal International*, *206*(2), 1009–1038. https://doi.org/10.1093/gji/ggw186

Pürschel, M., Gloaguen, R., & Stadler, S. (2013). Geothermal activities in the Main Ethiopian Rift: Hydrogeochemical characterization of geothermal waters and geothermometry applications (Dofan-Fantale, Gergede-Sodere, Aluto-Langano). *Geothermics*, *47*, 1–12. https://doi.org/10.1016/j.geothermics.2013.01.001

Regenspurg, S., Virchow, L., Wilke, F. D., Zimmer, M., Jolie, E., Hachenberger, A., et al. (2022). Origin and migration of fluoride in the area of the Aluto volcanic complex (Main Ethiopian Rift). *Applied Geochemistry*, *146*, 105403. https://doi.org/10.1016/j.apgeochem.2022.105403

Reinsch, T., Dobson, P., Asanuma, H., Huenges, E., Poletto, F., & Sanjuan, B. (2017). Utilizing supercritical geothermal systems: A review of past ventures and ongoing research activities. *Geothermal Energy*, *5*(1), 1–25. https://doi.org/10.1186/s40517-017-0075-y

Richter, C. F. (1935). An instrumental earthquake magnitude scale. *Bulletin of the Seismological Society of America*, *25*(1), 1–32. https://doi.org/10.1785/bssa0250010001

Roberts, N. S., Bell, A. F., & Main, I. G. (2015). Are volcanic seismic b-values high, and if so when? *Journal of Volcanology and Geothermal Research*, *308*, 127–141. https://doi.org/10.1016/j.jvolgeores.2015.10.021

Robertson, E., Biggs, J., Cashman, K., Floyd, M., & Vye-Brown, C. (2016). Influence of regional tectonics and pre-existing structures on the formation of elliptical calderas in the Kenyan Rift. *Geological Society, London, Special Publications*, *420*(1), 43–67. https://doi.org/10.1144/sp420.12

Roman, D. C., LaFemina, P. C., Bussard, R., Stephens, K., Wauthier, C., Higgins, M., et al. (2019). Mechanisms of unrest and eruption at persistently restless volcanoes: Insights from the 2015 eruption of Telica volcano, Nicaragua. *Geochemistry, Geophysics, Geosystems*, *20*(8), 4162–4183. https://doi.org/10.1029/2019gc008450

Rooney, T., Furman, T., Bastow, I., Ayalew, D., & Yirgu, G. (2007). Lithospheric modification during crustal extension in the Main Ethiopian Rift. *Journal of Geophysical Research*, *112*(B10). https://doi.org/10.1029/2006jb004916

Rooney, T. O., Furman, T., Yirgu, G., & Ayalew, D. (2005). Structure of the Ethiopian lithosphere: Xenolith evidence in the Main Ethiopian Rift. *Geochimica et Cosmochimica Acta*, *69*(15), 3889–3910. https://doi.org/10.1016/j.gca.2005.03.043

Saibi, H., Aboud, E., & Ehara, S. (2012). Analysis and interpretation of gravity data from the Aluto-Langano geothermal field of Ethiopia. *Acta Geophysica*, *60*(2), 318–336. https://doi.org/10.2478/s11600-011-0061-x

Samrock, F., Grayver, A., Dambly, M. L. T., Müller, M. R., & Saar, M. O. (2023). Geophysically guided well siting at the Aluto-Langano geothermal reservoir. *Geophysics*, *88*(5), WB105–WB114. https://doi.org/10.1190/geo2022-0617.1

Samrock, F., Grayver, A. V., Bachmann, O., Karakas, Ö., & Saar, M. O. (2021). Integrated magnetotelluric and petrological analysis of felsic magma reservoirs: Insights from Ethiopian rift volcanoes. *Earth and Planetary Science Letters*, *559*, 116765. https://doi.org/10.1016/j.epsl.2021.116765

Samrock, F., Grayver, A. V., Cherkose, B., Kuvshinov, A., & Saar, M. O. (2020). Aluto-Langano geothermal field, Ethiopia: Complete image of underlying magmatic-hydrothermal system revealed by revised interpretation of magnetotelluric data. In *World geothermal congress (wgc 2020+ 1)*.11054

Samrock, F., Grayver, A. V., Eysteinsson, H., & Saar, M. O. (2018). Magnetotelluric image of transcrustal magmatic system beneath the Tulu Moye geothermal prospect in the Ethiopian Rift. *Geophysical Research Letters*, *45*(23), 12–847. https://doi.org/10.1029/2018gl080333

Samrock, F., Kuvshinov, A., Bakker, J., Jackson, A., & Fisseha, S. (2015). 3-D analysis and interpretation of magnetotelluric data from the Aluto-Langano geothermal field, Ethiopia. *Geophysical Journal International*, *202*(3), 1923–1948. https://doi.org/10.1093/gji/ggv270

Sanjuan, B., Gourcerol, B., Millot, R., Rettenmaier, D., Jeandel, E., & Rombaut, A. (2022). Lithium-rich geothermal brines in Europe: An up-date about geochemical characteristics and implications for potential Li resources. *Geothermics*, *101*, 102385. https://doi.org/10.1016/j.geothermics.2022.102385

Searle, R., & Gouin, P. (1972). A gravity survey of the central part of the Ethiopian Rift Valley. *Tectonophysics*, *15*(1–2), 41–52. https://doi.org/10.1016/b978-0-444-41087-0.50009-9

Segall, P. (2013). Volcano deformation and eruption forecasting. *Geological Society*, *380*(1), 85–106. https://doi.org/10.1144/sp380.4

Shelly, D. R., Ellsworth, W. L., & Hill, D. P. (2016). Fluid-faulting evolution in high definition: Connecting fault structure and frequency-magnitude variations during the 2014 Long Valley Caldera, California, earthquake swarm. *Journal of Geophysical Research: Solid Earth*, *121*(3), 1776–1795. https://doi.org/10.1002/2015jb012719

Sigmundsson, F., Vadon, H., & Massonnet, D. (1997). Readjustment of the Krafla spreading segment to crustal rifting measured by satellite radar interferometry. *Geophysical Research Letters*, *24*(15), 1843–1846. https://doi.org/10.1029/97gl01934

Smith, J. D., White, R. S., Avouac, J.-P., & Bourne, S. (2020). Probabilistic earthquake locations of induced seismicity in the Groningen region, The Netherlands. *Geophysical Journal International*, *222*(1), 507–516. https://doi.org/10.1093/gji/ggaa179

Soosalu, H., Key, J., White, R. S., Knox, C., Einarsson, P., & Jakobsdóttir, S. S. (2010). Lower-crustal earthquakes caused by magma movement beneath Askja volcano on the north Iceland rift. *Bulletin of Volcanology*, *72*(1), 55–62. https://doi.org/10.1007/s00445-009-0297-3

Sparks, R., Annen, C., Blundy, J., Cashman, K., Rust, A., & Jackson, M. (2019). Formation and dynamics of magma reservoirs. *Philosophical Transactions of the Royal society A*, *377*(2139), 20180019. https://doi.org/10.1098/rsta.2018.0019

Stich, D., Ammon, C. J., & Morales, J. (2003). Moment tensor solutions for small and moderate earthquakes in the Ibero-Maghreb region. *Journal of Geophysical Research*, *108*(B3). https://doi.org/10.1029/2002jb002057

Stix, J. (2018). Understanding fast and slow unrest at volcanoes and implications for eruption forecasting. *Frontiers in Earth Science*, *6*, 56. https://doi.org/10.3389/feart.2018.00056

Stork, A. L., Verdon, J. P., & Kendall, J.-M. (2014). The robustness of seismic moment and magnitudes estimated using spectral analysis. *Geophysical Prospecting*, *62*(4), 862–878. https://doi.org/10.1111/1365-2478.12134

Stuart, G., Bastow, I., & Ebinger, C. (2006). Crustal structure of the northern Main Ethiopian Rift from receiver function studies. *Geological Society, London, Special Publications*, *259*(1), 253–267. https://doi.org/10.1144/gsl.sp.2006.259.01.20

Sturkell, E., & Sigmundsson, F. (2000). Continuous deflation of the Askja caldera, Iceland, during the 1983–1998 noneruptive period. *Journal of Geophysical Research*, *105*(B11), 25671–25684. https://doi.org/10.1029/2000jb900178

Styron, R., & Pagani, M. (2020). The GEM global active faults database. *Earthquake Spectra*, *36*(1_suppl), 160–180. https://doi.org/10.1177/8755293020944182

Tadesse, A. Z., Fontijn, K., Caricchi, L., Bégué, F., Gudbrandsson, S., Smith, V., et al. (2023). Pre-eruptive storage conditions and magmatic evolution of the Bora-Baricha-Tullu Moye volcanic system, Main Ethiopian Rift. *Lithos*, *442*, 107088. https://doi.org/10.1016/j.lithos.2023.107088

Tape, W., & Tape, C. (2012). A geometric comparison of source-type plots for moment tensors. *Geophysical Journal International*, *190*(1), 499–510. https://doi.org/10.1111/j.1365-246x.2012.05490.x

Tarantola, A., & Valette, B. (1982). Inverse problems= Quest for information. *Journal of Geophysics*, *50*(1), 159–170.

Taroni, M., Zhuang, J., & Marzocchi, W. (2021). High-definition mapping of the Gutenberg–Richter b-value and its relevance: A case study in Italy. *Seismological Research Letters*, *92*(6), 3778–3784. https://doi.org/10.1785/0220210017

Teklemariam, M., Battaglia, S., Gianelli, G., & Ruggieri, G. (1996). Hydrothermal alteration in the Aluto-Langano geothermal field, Ethiopia. *Geothermics*, *25*(6), 679–702. https://doi.org/10.1016/s0375-6505(96)00019-3

The ARGOS Project. (2012). ARGOS - Alutu and regional geophysical observation study. *International Federation of Digital Seismograph Networks*. https://doi.org/10.7914/SN/XM_2012

Troise, C., De Natale, G., Schiavone, R., Somma, R., & Moretti, R. (2019). The Campi Flegrei caldera unrest: Discriminating magma intrusions from hydrothermal effects and implications for possible evolution. *Earth-Science Reviews*, *188*, 108–122. https://doi.org/10.1016/j.earscirev.2018.11.007

Uchide, T., & Imanishi, K. (2018). Underestimation of microearthquake size by the magnitude scale of the Japan Meteorological Agency: Influence on earthquake statistics. *Journal of Geophysical Research: Solid Earth*, *123*(1), 606–620. https://doi.org/10.1002/2017jb014697

Vavryčuk, V. (2001). Inversion for parameters of tensile earthquakes. *Journal of Geophysical Research*, *106*(B8), 16339–16355. https://doi.org/10.1029/2001jb000372

Vavryčuk, V. (2002). Non-double-couple earthquakes of 1997 January in West Bohemia, Czech Republic: Evidence of tensile faulting. *Geophysical Journal International*, *149*(2), 364–373. https://doi.org/10.1046/j.1365-246x.2002.01654.x

Vavryčuk, V. (2015). Moment tensor decompositions revisited. *Journal of Seismology*, *19*(1), 231–252. https://doi.org/10.1007/s10950-014-9463-y

Weinand, J. M., Vandenberg, G., Risch, S., Behrens, J., Pflugradt, N., Linßen, J., & Stolten, D. (2023). Low-Carbon Lithium extraction makes deep geothermal plants cost-competitive in future energy systems. *Advances in Applied Energy*, *11*, 100148. https://doi.org/10.1016/j.adapen.2023.100148

Wessel, P., Luis, J. F., Uieda, L. a., Scharroo, R., Wobbe, F., Smith, W. H., & Tian, D. (2019). The generic mapping tools version 6. *Geochemistry, Geophysics, Geosystems*, *20*(11), 5556–5564. https://doi.org/10.1029/2019gc008515

Whaler, K., & Hautot, S. (2006). The electrical resistivity structure of the crust beneath the northern Main Ethiopian Rift. *Geological Society*, *259*(1), 293–305. https://doi.org/10.1144/gsl.sp.2006.259.01.22

Wilks, M., Ayele, A., Kendall, J.-M., & Wookey, J. (2017). The 24th January 2016 Hawassa earthquake: Implications for seismic hazard in the Main Ethiopian Rift. *Journal of African Earth Sciences*, *125*, 118–125. https://doi.org/10.1016/j.jafrearsci.2016.11.007

Wilks, M., Kendall, J.-M., Nowacki, A., Biggs, J., Wookey, J., Birhanu, Y., et al. (2017). Seismicity associated with magmatism, faulting and hydrothermal circulation at Aluto Volcano, Main Ethiopian Rift. *Journal of Volcanology and Geothermal Research*, *340*, 52–67. https://doi.org/10.1016/j.jvolgeores.2017.04.003

Wilks, M., Rawlinson, N., Kendall, J.-M., Nowacki, A., Biggs, J., Ayele, A., & Wookey, J. (2020). The coupled magmatic and hydrothermal systems of the restless Aluto caldera, Ethiopia. *Frontiers in Earth Science*, *8*, 579699. https://doi.org/10.3389/feart.2020.579699

Wittlinger, G., Herquel, G., & Nakache, T. (1993). Earthquake location in strongly heterogeneous media. *Geophysical Journal International*, *115*(3), 759–777. https://doi.org/10.1111/j.1365-246x.1993.tb01491.x

Woldegabriel, G., Aronson, J. L., & Walter, R. C. (1990). Geology, geochronology, and rift basin development in the central sector of the Main Ethiopia Rift. *Geological Society of America Bulletin*, *102*(4), 439–458. https://doi.org/10.1130/0016-7606(1990)102<0439:ggarbd>2.3.co;2

Wuletawu, H., Alemu, A., Nigussie, W., Mickus, K., Keir, D., Wendwesen, S., & Wassihun, S. (2024). The subsurface anatomy of a mid-upper crustal magmatic intrusion zone beneath the Boku volcanic complex, Main Ethiopian Rift inferred from gravity data. *Journal of Volcanology and Geothermal Research*, *452*, 108133. https://doi.org/10.1016/j.jvolgeores.2024.108133

Wyss, M. (1973). Towards a physical understanding of the earthquake frequency distribution. *Geophysical Journal of the Royal Astronomical Society*, *31*(4), 341–359. https://doi.org/10.1111/j.1365-246x.1973.tb06506.x

Wyss, M., Klein, F., Nagamine, K., & Wiemer, S. (2001). Anomalously high b-values in the South Flank of Kilauea volcano, Hawaii: Evidence for the distribution of magma below Kilauea's East rift zone. *Journal of Volcanology and Geothermal Research*, *106*(1–2), 23–37. https://doi.org/10.1016/s0377-0273(00)00263-8

Yemane, T., Hudson, T. S., Kendall, J. M., Blundy, J., Tadesse, A. Z., Hammond, J. O., et al. (2025). Interconnectivity of Magmatic and hydrothermal systems of Aluto Volcano in the Main Ethiopian Rift Inferred from seismicity (version 1) [Dataset]. *Zenodo*. https://doi.org/10.5281/zenodo.15243910

Yirgu, G., Ebinger, C. J., & Maguire, P. (2006). The Afar volcanic province within the East African Rift System: Introduction. *Geological Society, London, Special Publications*, *259*(1), 1–6. https://doi.org/10.1144/gsl.sp.2006.259.01.01

Zhao, M., Langston, C. A., Nyblade, A. A., & Owens, T. J. (1997). Lower-crustal rifting in the Rukwa graben, East Africa. *Geophysical Journal International*, *129*(2), 412–420. https://doi.org/10.1111/j.1365-246x.1997.tb01592.x